



NITROUS OXIDE (N₂O) in MACQUARIE HARBOUR, TASMANIA

Maxey, Johnathan Daniel^{1,2}, Neil D. Hartstein², Hermann W. Bange³, Moritz Müller¹

5 ¹Faculty of Engineering, Computing and Science, Swinburne University of Technology, Kuching 93350, Malaysia

²ADS Environmental Services, Kota Kinabalu, Sabah, 88400, Malaysia

³GEOMAR Helmholtz Centre for Ocean Research Kiel, Wischhofstr. 1-3, 24148 Kiel, Germany

Correspondence to: Johnathan Daniel Maxey, Neil D. Hartstein, Hermann W. Bange, and Moritz Müller

Abstract. Fjord-like estuaries are hotspots of biogeochemical cycling due to steep physicochemical gradients.
10 The spatiotemporal distribution of nitrous oxide (N₂O) within many of these systems is poorly described, especially in the southern hemisphere. The goal of this study is to describe the spatiotemporal distribution of N₂O within a southern hemisphere fjord-like estuary, describe the main environmental drivers of this distribution, the air/sea flux of N₂O, and the main drivers of N₂O production. Cruises were undertaken in Macquarie Harbour, Tasmania to capture N₂O concentrations and water column physicochemical profiles in
15 winter (July 2022), spring (October 2022), summer (February 2023), and autumn (April 2023). N₂O samples were collected at one depth at system end members, and at 5 depths at 4 stations within the harbour.

Results indicate that N₂O is consistently supersaturated (reaching 170% saturation) below the system's freshwater lens where oxygen concentrations are often hypoxic, but infrequently anoxic. In the surface lens,
20 levels of N₂O saturation vary with estimated river flow and with proximity to the system's main freshwater endmember. The linear relationship between AOU and ΔN₂O saturation indicates that nitrification is the process generating N₂O in the system. When river flow was high (July and October 2022), surface water N₂O was undersaturated (as low as 70%) throughout most of the harbour.

25 When river flow was low (February and April 2023) N₂O was observed to be supersaturated at most stations. Calculated air/sea fluxes of N₂O indicated that the system is generally a source of N₂O to the atmosphere under weak river flow conditions and a sink during strong river flow conditions. The diapycnal flux was a minor contributor to surface water N₂O concentrations, and subhalocline N₂O is intercepted by the riverine surface lens and transported out of the system to the ocean during strong river flow conditions. In a changing climate,
30 Western Tasmania is expected to receive higher winter rainfall and lower summer rainfall which may augment the source and sink dynamics of this system by enhancing the summer / autumn efflux of N₂O to the atmosphere.

This study is the first to report observations of N₂O distribution, generation processes, and estimated diapycnal / surface N₂O fluxes from this system.



35 **1. Introduction**

Despite the fact that fjords and fjord-like estuaries represent only a small portion of the coastal area worldwide they are responsible for sequestering 11% of the global organic carbon (C) burial along terrestrial margins (Smith *et al.*, 2015; Bianchi *et al.*, 2018, 2020). These systems are significant sources of greenhouse gasses (GHG) to the atmosphere (Wilson *et al.*, 2020; Rosentreter *et al.*, 2023; Bange *et al.*, 2024). Many are heavily stratified with strong water column physicochemical gradients (Acuña-González *et al.*, 2006; Inall and Gillibrand, 2010; Hartstein *et al.*, 2019; Salamena *et al.*, 2021, 2022; Maxey *et al.*, 2022). These gradients can be influenced by mesoscale climate drivers like NAO and SAM (see Austin and Inall 2002; Gillibrand *et al.*, 2005; Maxey *et al.*, 2022) and local scale drivers like fresh water input and marine intrusions (Inall and Gillibrand 2010; Hartstein *et al.*, 2019; Maxey *et al.*, 2020; Salamena *et al.*, 2022).

45 Nitrous oxide (N₂O) is a potent GHG whose increased presence in the atmosphere is primarily driven by emissions from agricultural soils with an increased presence in poorly oxygenated marine systems (Laffoley and Baxter 2019; Ji *et al.*, 2020; Wilson *et al.*, 2020; Wan *et al.*, 2022; Orif *et al.*, 2023). With a global warming potential nearly 300 times that of CO₂ (Myhre *et al.*, 2013; Etminan *et al.*, 2016; Eyring *et al.*, 2021; Forster *et al.*, 2021) N₂O is a key focus of climate studies especially regarding ozone layer depletion. N₂O is a precursor to NO, and a major ozone depleting substance in the atmosphere (Nevison and Holland, 1997; Ravishankara *et al.*, 2009; Portmann *et al.*, 2012). N₂O production occurs through the microbially mediated processes of ammonia oxidation, nitrite (NO₂⁻) reduction, and nitrate (NO₃⁻) reduction (Kuypers *et al.*, 2018). N₂O production in marine systems is governed by environmental conditions such as dissolved oxygen (DO) availability, ammonium (NH₄⁺) availability, light availability, temperature (*e.g.* Raes *et al.*, 2016), pH (*e.g.* Breider *et al.*, 2019), and microbial community composition (*e.g.* Wu *et al.*, 2020).

Estuarine systems have disproportionately high biological productivity relative to other marine systems (Walinsky *et al.*, 2009; Gilbert *et al.*, 2010; Bianchi *et al.*, 2018, 2020). This also applies to N₂O dynamics with approx. 33% of marine N₂O emissions coming from estuaries (Bange *et al.*, 1996; Seitzinger *et al.*, 2000; Murry *et al.*, 2015; Reading, 2022; Rosentreter *et al.*, 2023). Estuaries can act as net sinks (Maher *et al.*, 2016; Wells *et al.*, 2018) and sources (De Bie *et al.*, 2002; Zhang *et al.*, 2010; Sánchez-Rodríguez *et al.*, 2022) of N₂O depending on factors controlling air/sea fluxes, waterbody/atmospheric concentrations (Wells *et al.*, 2018; Bange *et al.*, 2019), land use modification (Reading *et al.*, 2020; Chen *et al.*, 2022), and even the presence of microplastics (Chen *et al.*, 2022). Despite the advancements made thus far, our understanding of marine N₂O distribution and atmospheric emissions needs improvement (Bange *et al.*, 2024), especially in southern hemisphere fjord-like systems (Yevenes *et al.*, 2017). Much of the current uncertainty lies with a lack of in-situ data describing seasonal N₂O dynamics to constrain global emissions models (Bange *et al.*, 2019).

70 The purpose of this study was (1) to investigate the distribution and seasonal variability of N₂O concentrations and emissions in a southern hemisphere fjord-like estuary and (2) to decipher the major physical and biological drivers of the N₂O emissions.



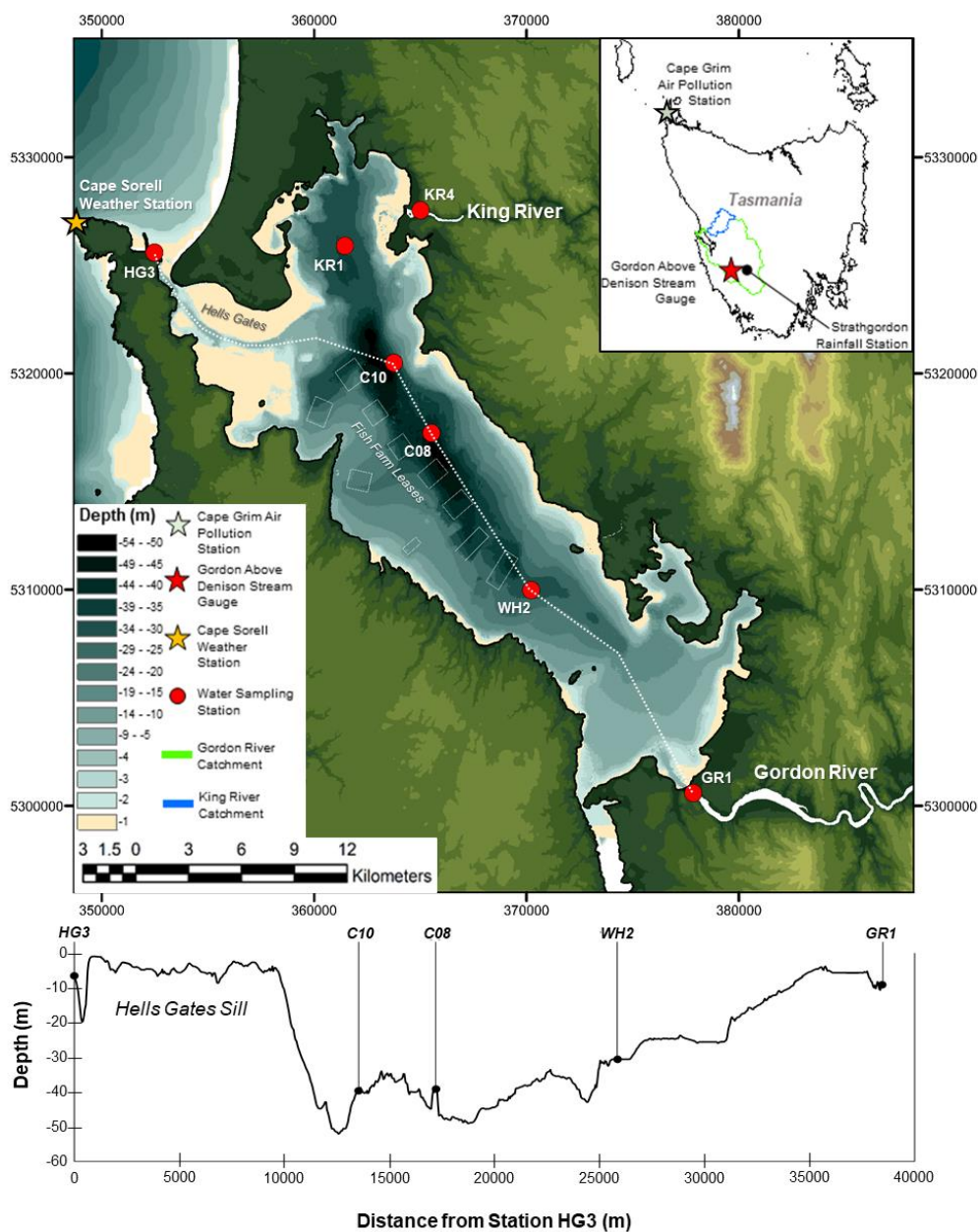
2. Methods

75 2.1 Study Area

Macquarie Harbour is a southern hemisphere fjord-like estuary located on Tasmania's west coast (**Figure 1**). The harbour is oriented NW by SE, and is approximately 33 km long, 9 km wide, with a surface area of 276 km². The mouth of the harbour is constricted by a shallow (4-8m), long (14km) sill known as "Hells Gates". Hells Gates muffles tidal forcing resulting in harbour water levels primarily determined by river flow and wind set up
80 (**Hartstein et al., 2019**). The morphology of this system results in sharp gradients of DO, salinity, and temperature which are seasonally dependant (**Creswell et al., 1989; Hartstein et al., 2019; Maxey et al., 2022**). In surface waters DO concentrations are nearly always in equilibrium with the air but decrease sharply through the halocline (~8m to 15m). Subhalocline layers (~15m to a few meters from the bottom) are observed to be below 62.5 μM more than 50% of the time (*see* **Maxey et al., 2022**). Near the seabed, episodic marine intrusions
85 (deep water renewal) refresh the supply of DO. In the upper reaches of the harbour marine intrusions are much less common (*see* **Hartstein et al., 2019; Maxey et al., 2022**). In these areas the DO concentration falls below 31 μM nearly a third of the time (**Maxey et al., 2022**).

Like many fjord-like estuaries, the distribution of DO is driven by multiple physical and biological processes
90 whose relative importance depends on position along the estuarine axis as well as water column depth (**Hartstein et al., 2019** and **Maxey et al., 2017, 2020, 2022**). There is almost no DO produced below the halocline (8m to 12m deep) as the overlying freshwater lens is high in chromophoric dissolved organic matter (CDOM) limiting light available to primary producers in the surface water layers (within 3m) (**Maxey et al., 2017, 2020**). Basin water oxygen concentrations and salinity are largely influenced by advection of marine water
95 over Hells Gates (**Andrewartha and Wild-Allen 2017; Hartstein et al., 2019; Maxey et al., 2022**). This process is driven by low atmospheric pressure, sustained NW winds, and low catchment rainfall which itself is influenced by Southern Annular Mode (SAM) (**Hartstein et al., 2019; Maxey et al., 2022**). Hydrodynamic and oxygen tracer numerical simulations of the harbour by **Andrewartha and Wild-Allen (2017)** support measurements by **Maxey et al. (2022)** which show that basin water residence times and basin water oxygen
100 concentrations are tied to the flow conditions of the freshwater endmembers. In their model basin water tracer concentrations were reduced by half in approximately 65 days during low river flow conditions (approximately 70 days at the surface) and in approximately 110 days during normal flow conditions (approximately 40 days at the surface).

105 The main source of freshwater to the harbour is located on its southeast end (the Gordon River) and drains a nearly pristine catchment (including the Franklin River) of approximately 5,682 km² (**Macquarie Harbour Dissolved Oxygen Working Group, 2014; Fig 1**). The Gordon River discharges an estimated 180,000 tons organic carbon (OC) per year (**Maxey et al., 2020, 2022**) into the estuary. It should be noted that this area receives the some of the highest rainfall (more than 2,500 mm year⁻¹) volume in Australia (**Dey et al., 2019**). The
110 King River, located on the harbour's northern end, is the second largest contributor of fresh water to the estuary and drains a catchment area of 802 km². Unlike the Gordon River, the King River has a history of receiving treated mining (*e.g.* copper) effluent and transporting this to the harbour (**Carpenter et al., 1991; Teasdale et al., 2003**).



115 **Figure 1: Macquarie Harbour, Tasmania.** Water sampling stations shown with red circles; Cape Grim Air Pollution
 monitoring station shown as a green star (see inset map). Cape Sorell Weather Station shown as an orange star.
 Gordon Above Denison stream gauge shown as a red star (see inset map). Aquaculture lease boundaries are shown as
 hollow rectangles. Lease locations are sourced from Land Information Systems Tasmania (LISTmap -
 https://maps.thelist.tas.gov.au/). Station names reflect general harbour locations where KR1 indicates King River 1;
 120 C10 and C08 indicate Central Harbour 10 and 08 respectively; WH2 indicates World Heritage Area 2; and GR1
 indicates Gordon River station 1. Coordinates are displayed in GDA_1994_MGA_Zone_55. Bathymetry through the
 system shown as a dashed line, note that this track excludes stations KR4 and KR1.



2.2 Experimental Design

125 N₂O distribution was assessed by collecting water samples across 7 stations, including the harbour's
endmembers (mouths of the Gordon and King Rivers as well as the harbour mouth at Hells Gates Inlet; *see*
Figure 1 and **Table 1**) and stations along the longitudinal axis of the harbour where the deepest basins are
located (named KR1, C10, C08, and WH2). Samples collected at endmember stations were collected from a
single depth as these stations are shallow. Samples in the harbour body were collected at 5 depths from the
130 surface (2m) to approx. 1m from the seabed. Collection campaigns were conducted in July 2022, October 2022,
February 2023, and April 2023. At each station and depth three replicate vials (n = 3) were collected for the
determination of N₂O concentration.

2.3 Field Sampling

135 At each station, water quality sonde profiles were collected from the surface to the seabed at 1 meter intervals
using a YSI EXO-1 equipped with optical DO (accuracy from 0 to 625 $\mu\text{M} \pm 3 \mu\text{M}$ or 1% of reading whichever
is greater; precision is 0.03 μM), salinity (accuracy ± 0.1 or 1% of reading whichever is greater; precision is
0.01), temperature (accuracy is ± 0.15 °C; precision is 0.01 °C), and depth sensors. Sonde calibration was
checked and corrected (when needed) each sampling period.

140

Water samples were collected at various depths (see **Table 1**) using a 5 L Niskin bottle sampler. Water sample
parameters include dissolved Total Ammoniacal N ($\text{NH}_3 + \text{NH}_4^+$) (TAN), NO_3^- , and N₂O. N₂O samples were
collected in triplicate immediately after retrieval of the Niskin bottle by transferring water from the bottle
through silicone tubing into a 20 mL borosilicate vial. Sample water was added to the vial by placing the tubing
145 at the bottom and allowing the vial to overflow several volumes before sealing with a butyl rubber stopper and
aluminium crimp. After ensuring the sample vial is bubble free, 50 μL of saturated mercury chloride (HgCl_2)
solution was injected into the sample to arrest biological activity. All N₂O samples were shipped to GEOMAR in
Kiel, Germany for analysis. Samples were measured in July/August 2023 within 4 to 12 months after sampling
and were not affected by the storage time (**Wilson et al., 2018**).

150

Water collected for dissolved inorganic nitrogen (N) was filtered immediately using 0.45 μm polyethersulfone
syringe filters (Whatman Puradisc). Samples were stored in a chilled dark container until being transported to
Analytical Services Tasmania in Hobart, Australia for analysis. Dissolved Total TAN and NO_3^- were analysed
using a Lachat Flow Injection Analyser. TAN and NO_3^- analyses used methods based on APHA Standard
155 methods (2005) 4500-NH₃ H (reporting limit 0.005 mg L⁻¹) and 4500 - NO_3^- L⁻¹ (reporting limit 0.002 mg L⁻¹).

Table 1: Sampling stations showing coordinates, parameters, and sampling depth (in meters).

Station	Station Depth (m) (MSL)	Dissolved Oxygen Salinity Temperature	N ₂ O	TAN (NH ₃ + NH ₄ ⁺)	NO ₃ ⁻
HG3 352484, 5325594	8	Every Meter	5m	5m	5m



KR4 365018, 5327550	3	1m	1m	1m	1m
KR1 361316, 5325972	36	Every Meter	2, 12, 20, 30, 35m	2, 12, 20, 30, 35m	2, 12, 20, 30, 35m
C10 363708, 5320464	44	Every Meter	2, 12, 20, 30, 42m	2, 12, 20, 30, 42m	2, 12, 20, 30, 42m
C08 365489, 5317238	47	Every Meter	2, 15, 25, 35, 45m	2, 15, 25, 35, 45m	2, 15, 25, 35, 45m
WH2 370218, 5309894	32	Every Meter	2, 12, 20, 25, 30m	2, 12, 20, 25, 30m	2, 12, 20, 25, 30m
GR1 377784, 5300603	12	Every Meter	10m	10m	10m

160 2.4 Analysis of Rainfall and River Loading Estimation

River loading and rainfall were analysed using methods presented in **Maxey *et al.* (2022)** where rainfall and stream gauge data were collected from the Gordon River catchment, Strathgordon rainfall gauge station and the Gordon Above Denison (GAD) stream gauge (**Figure 1**). The rainfall and flow metrics computed include the average daily rainfall over a 20-day period prior to sampling; total accumulated rainfall 20,10, 5, and 3 days prior to sampling; estimated Gordon River flow into the estuary; and measured flow at the GAD stream gauge.

Gordon River flow was estimated by scaling daily rainfall to the size of the catchment and assuming a rainfall and runoff coefficient of 0.70 adopted from a neighbouring catchment with similar land cover, geology, and slope (**Willis, 2008**). Additional streamflow from Gordon River dam releases was estimated by subtracting scaled rainfall contributions to river flow measured at the GAD stream gauge. This flow was added to the estimated runoff entering the harbour. Rainfall and flow data were provided by the Australian Bureau of Meteorology (BOM).

NO_3^- and TAN loading was estimated by multiplying the measured concentration of each parameter at station GR1 (*see Figure 1 and Table 1*) by the estimated Gordon River flow.

2.5 Analysis of Water Column N_2O Concentrations, Air/Sea Flux, and Diapycnal Flux

2.5.1 Determination of N_2O Concentrations

Water samples were analysed for N_2O using the static-headspace equilibration method followed by gas chromatographic separation (HP Agilent 5890) and detection with an electron capture detector (ECD) as described in **Bange *et al.*, (2019)**, **Bastian (2017)**, and **Kallert (2017)**. The concentrations of N_2O in the samples was calculated with the following equation (**Equation 1; see Bange *et al.*, 2006**):



Equation 1

$$C_{\text{obs}} = \frac{x' PV_{\text{hs}}}{RTPV_{\text{wp}}} + X'\beta P$$

185 C_{obs} is the concentration (nmol L⁻¹) of N₂O in the water sample; x' is the measured dry mole fraction of N₂O in the sample vial's headspace; P is the ambient pressure set to 1 atm; V_{hs} and V_{wp} are the volumes of the headspace in the vial and water in the vial; R is the gas constant; T is the temperature during equilibrium; and β is the solubility of N₂O (Weiss and Price, 1980). The mean relative error of the concentration values obtained was 2.4% (± 0.16).

190

2.5.2 Estimation of N₂O Air/Sea Fluxes and N₂O Saturations

N₂O air/sea fluxes (F in $\mu\text{mol m}^{-2} \text{d}^{-1}$) were estimated using equations from Zhang *et al.*, (2010) and Bange *et al.*, (2019) (Equation 2) Where:

195 Equation 2

$$F = K * (C_{\text{obs}} - C_{\text{eq}})$$

C_{obs} is the measured concentration (nmol L⁻¹) of N₂O in the water sample; C_{eq} is the air-equilibrated seawater N₂O concentration, calculated for in situ temperature and salinity using the solubility data of Weiss and Price (1980). K is the gas transfer velocity, which in the absence of direct measurements can be expressed as a function of the wind speed and the Schmidt Number (Sc). For this study we sourced daily average wind speed from the Cape Sorrel Weather Station at the northern end of Macquarie Harbour (<http://www.bom.gov.au/climate/data/index.shtml> station ID 097000; see Figure 1 for station location). K was estimated using relationships in Raymond and Cole (2001). Fluxes at Macquarie Harbour's endmember stations used K values that account for additional forcings like bottom shear (see Raymond and Cole 2001; Zappa *et al.*, 2003; Abril and Borges 2004, Beaulieu *et al.*, 2012; Rosentreter *et al.*, 2021). Deeper stations in the harbour's main body (*i.e.* KR1, C10, C08, WH2) have surface layers which are separated from the seabed by more than 10 meters. A wind-based K_{600} estimator was used to estimate air-sea flux in those locations (see Raymond and Cole 2001). Atmospheric N₂O for this estimation was sourced from monthly mean baseline greenhouse gas mole fractions measured at the Kennaook / Cape Grim Baseline Air Pollution Station, located in north west Tasmania. This station measures atmospheric N₂O using a gas chromatograph (GC) equipped with an ECD (<https://www.csiro.au/en/research/natural-environment/atmosphere/latest-greenhouse-gas-data>). N₂O saturation (in %) were computed as N₂O saturation = 100 * $C_{\text{obs}} * C_{\text{eq}}^{-1}$.

200
205
210

2.5.3 Estimation of Diapycnal N₂O Flux

215 N₂O diapycnal fluxes (F_{dia} ; Equation 3) from basin waters (sample depths of 20m or 25m) to the harbour's surface lens (sample depths of 2m) were estimated as:



Equation 3

$$F_{\text{dia}} = K_{\rho} \frac{d[\text{N}_2\text{O}]}{dz}$$

Where z is depth. Diapycnal diffusivity (K_{ρ} ; **Equation 4**) was computed with the local buoyancy frequency (N^2), Γ set to 0.2 (Osborn 1980), and ε the dissipation rate of turbulent kinetic energy assumed to be on the upper end of values for the mixing zone of stratified systems 1×10^{-5} (Arneborg *et al.*, 2004; Mickett *et al.*, 2004; Fer *et al.*, 2006).

Equation 4

$$K_{\rho} = \Gamma \frac{\varepsilon}{N^2}$$

2.6 Data Analysis

The relationships between N_2O saturation and water quality parameters such as DO concentration, salinity, temperature, nitrate, and ammonium concentrations were analysed using Pearson correlation. The effects of season and depth on N_2O saturation at each sampling station was tested using a 2-way ANOVA. The relationship between rainfall / river flow metrics from the Gordon River and surface water N_2O saturation / N_2O air/sea flux at each station was analysed using Pearson correlation.



3. Results

3.1 Rainfall and River Loading

235 Twenty-day rainfall accumulation ranged from a low of 117 mm in July 2022 to a high of 139 mm in April 2023 with no detectable seasonal differences (*see* **Figure 2A**). Average daily rainfall was similar across all months and ranged from 5.12 (\pm 2.57) mm in July 2022 to 5.79 (\pm 3.03) mm in October 2022 (*see* **Figure 2B**). As observed with accumulation metrics no seasonal differences were detected.

240 Estimated flow at the Gordon River mouth and GAD stream gauge were greater in July and October 2022 than February and April 2023 (**Figure 2C**). At the GAD stream gauge, average flows were observed to decrease during the study period. Greatest flow was observed in winter (July 2022) at 107.6 (\pm 15.9) m³ s⁻¹ and lowest in autumn (April 2023) at 30.5 (\pm 2.2) m³ s⁻¹ (**Figure 2D**).

245 Estimated NO₃⁻ and TAN loading varied with NO₃⁻ loads of 1.69 tonnes day⁻¹ observed in July 2022, dipping to 0.31 tonnes day⁻¹ in October 2022, and then rising again to 1.77 and 2.77 tonnes day⁻¹ in February and April 2023 (**Figure 2E**). TAN loading mirrored this pattern with peaks occurring in October 2022 and February 2023 and lows occurring in July 2022 and April 2023. Patterns in N₂O loading from the Gordon River were similar to those observed for NO₃⁻ (**Figure 2F**).

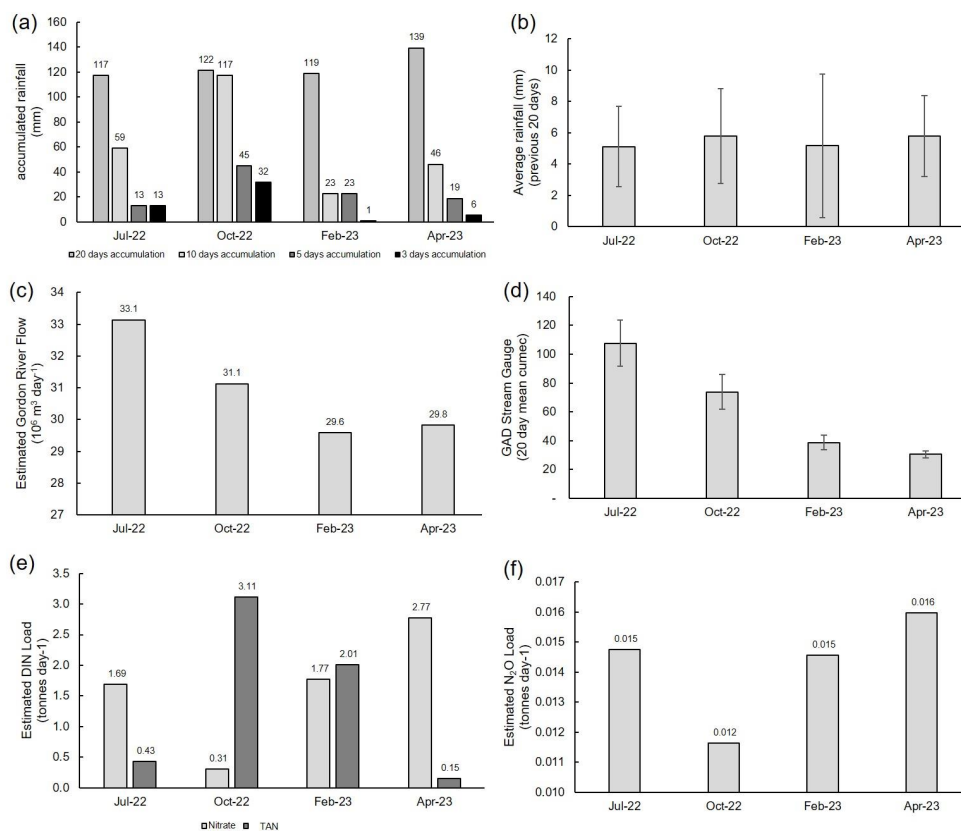
250

3.2 Water Column Physicochemical Profiles

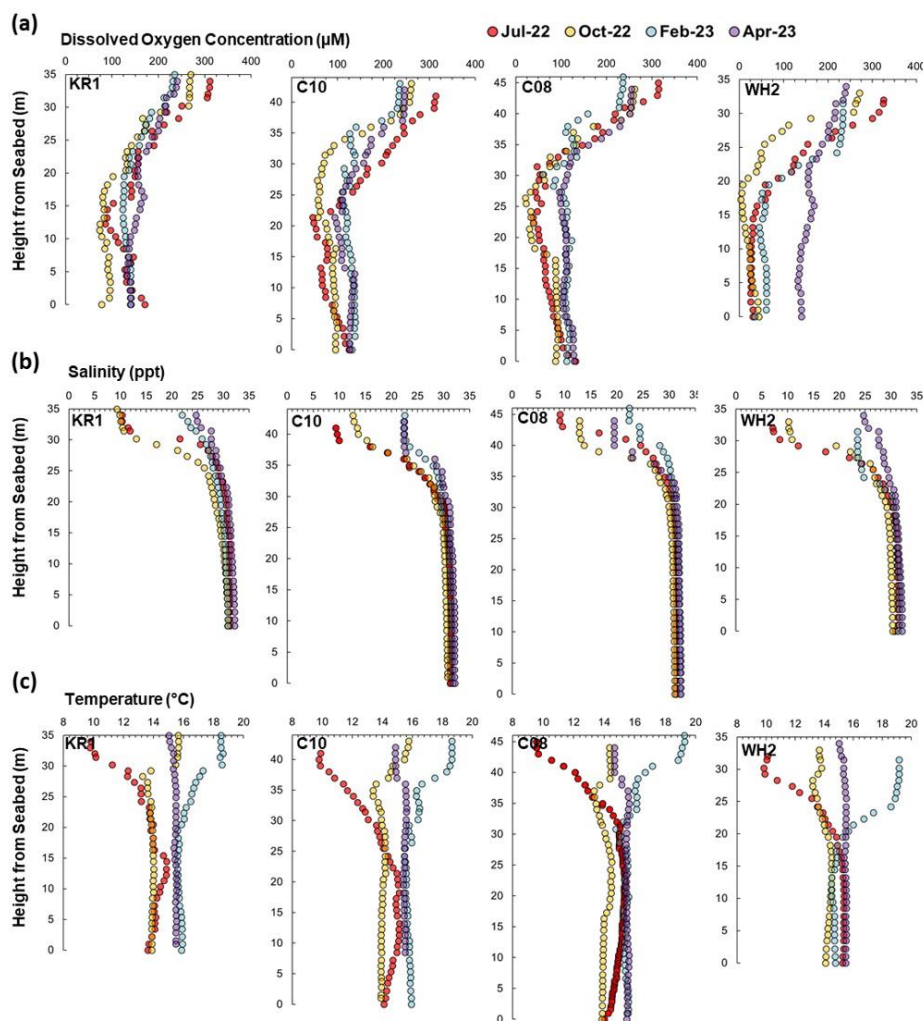
DO profiles at the stations located within the main body of the harbour show a well oxygenated surface layer that rapidly attenuates with depth (**Figure 3A**) through the halocline (**Figure 3B**). There is a prominent riverine surface lens in the main harbour extending to depths of up to 8m depending on sampling period and location within the estuary. Salinity in the surface waters was lower in July and October 2022 (6 to 13) than February and April 2023 (greater than 20). Below the halocline salinity ranged from approx. 28 to 32.

The DO gradient between the surface and subhalocline waters was steeper in October relative to July 2022 with October 2022 DO concentrations approaching single digits (3.1 μ M) at station WH2, nearest the Gordon River mouth (*see* **Figure 1**). In general, the subhalocline concentrations of DO were lower with proximity to the Gordon River mouth. The temperature of the freshwater surface layer ranged from about 9 °C to 19 °C, but showed little variation below the halocline where temperature ranged between 13 °C to 16 °C (**Figure 3C**).

260



265 **Figure 2: Rainfall and estimated Gordon River loading estimates for each sampling event. A) accumulated rainfall (mm) 10, 5, and 3 days prior to each sampling event; B) average (mean) daily rainfall over a 20 day period prior to each sampling event; C) estimated Gordon River Flow into the harbour in millions of m³ day⁻¹; D) daily mean flow (m³ sec⁻¹) over previous 20 days prior to sampling (\pm standard error) at the Gordon Above Denison Stream Gauge; E) estimated nitrate and ammonium loads entering the harbour from the Gordon River; F) estimated N₂O load (tonnes day⁻¹) entering the harbour from the Gordon River.**



270

Figure 3: Dissolved oxygen (μM) (Row A), salinity (Row B), and temperature ($^{\circ}\text{C}$) (Row C) profiles (referencing height from seabed) collected at stations KR1, C10, C08, and WH2 in July 2022 (red dots), October 2022 (yellow dots), February 2023 (blue dots), and April 2023 (purple dots). Measurements were made every 1 meter.

275

3.3 N_2O Distribution

At each harbour station, depth and season (and their interaction) significantly impacted N_2O saturation (two-way ANOVA, $\alpha = 0.05$, degree of freedom (*d.f.*) = 59). At 2 m, N_2O saturation was observed to be below 100% at all stations in July 2022 (Figure 4) and at stations KR1, C10, and C08 in October 2022. In February and April 2023 N_2O saturation in the harbour was above 100% through the water column except in KR1 surface waters. The maximum N_2O concentrations were observed in the subhalocline. Among the subhalocline observations the maximum N_2O concentrations (reaching over 170%) were observed at the base of the Hells Gates sill at station C10 in October 2022.

280



All endmember N₂O concentrations were undersaturated in July 2022. In October, stations KR1 and HG3 were observed to be approx. 100% saturated but N₂O at station GR1 was undersaturated. In February and April 2023
285 N₂O concentrations were supersaturated at all endmember stations. There were statistically significant linear correlations between N₂O saturation and salinity ($r = 0.494$; $p = 5.5 \times 10^{-7}$, $n = 92$), temperature ($r = 0.391$; $p = 1.2 \times 10^{-4}$, $d.f. = 90$), DO concentration ($r = -0.563$; $p = 5.2 \times 10^{-9}$, $d.f. = 90$), and nitrate concentration ($r = 0.559$; $p = 6.9 \times 10^{-9}$, $d.f. = 90$) in the harbour stations (**Figure 5**). The correlation between N₂O saturation and the TAN concentration however was not statistically significant ($r = 0.174$; $p = 0.31$, $d.f. = 34$).

290

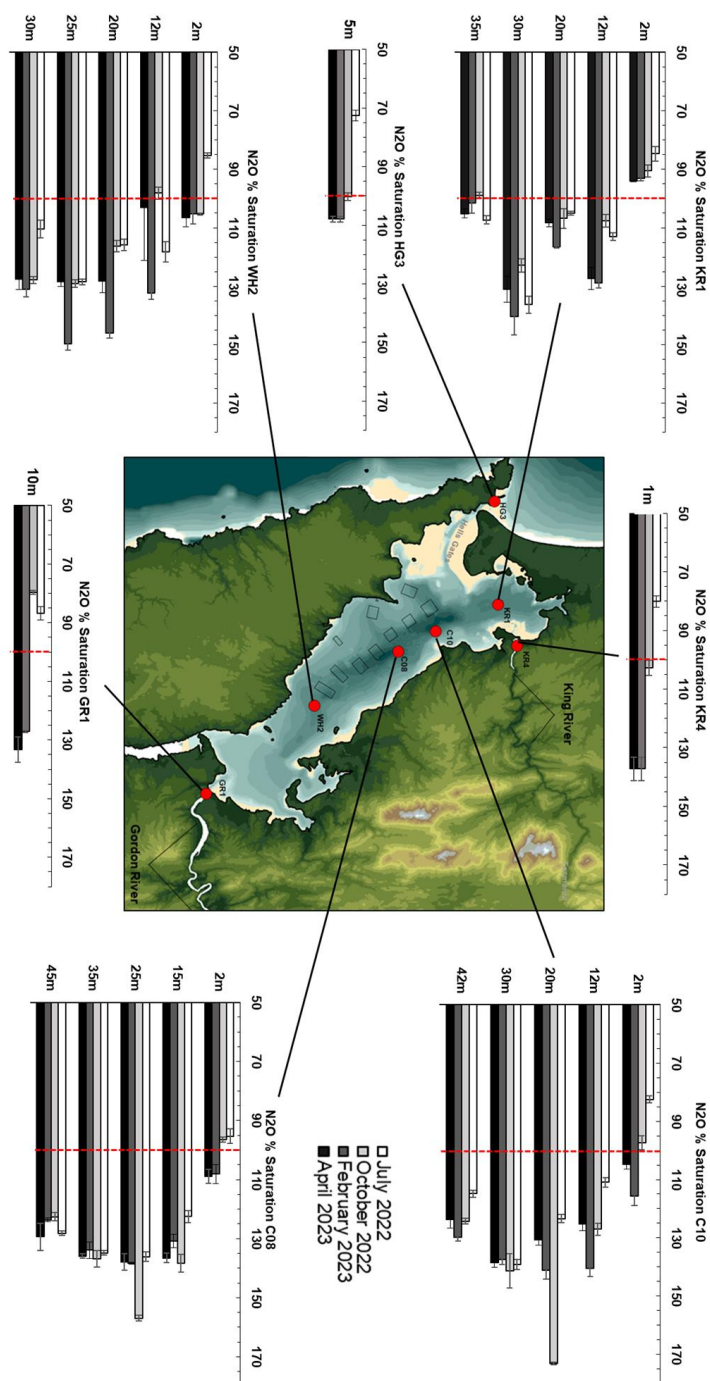
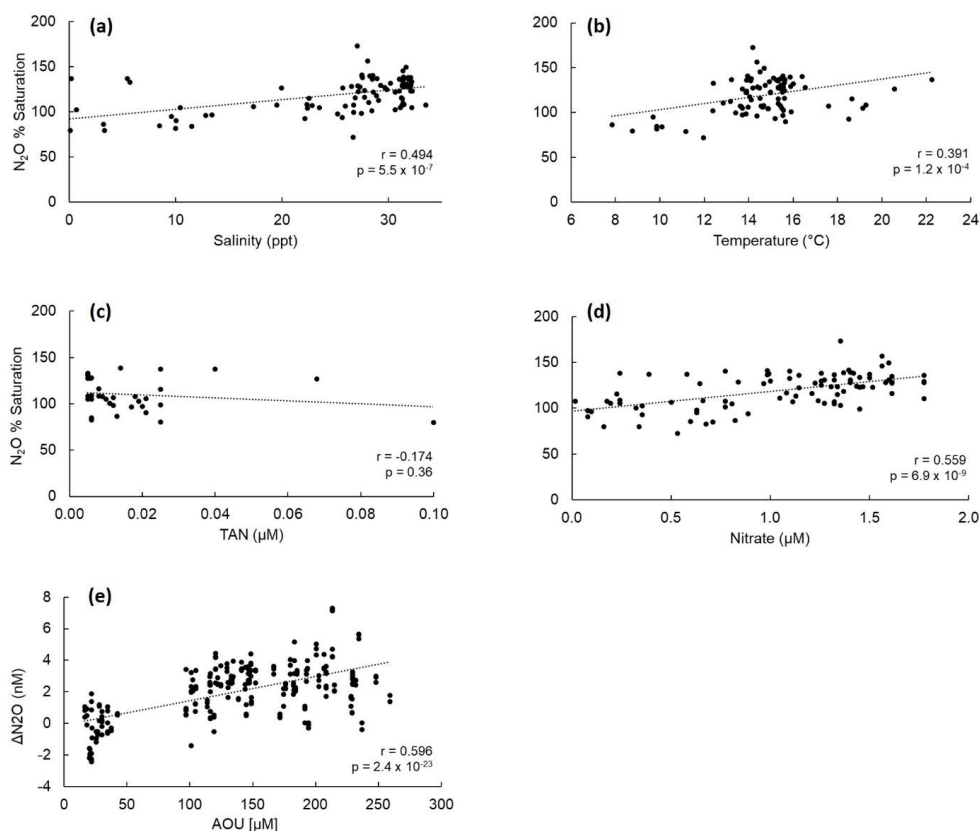


Figure 4: Mean (\pm standard error) N_2O % saturation observed at each sampling station, with depth, and across seasons. Note that a red dashed line indicating 100% at the time of sampling has been placed on each panel for reference.



295

Figure 5: Correlation between N₂O % Saturation observed across the harbour and A) Salinity, B) Temperature, C) Total Ammoniacal Nitrogen (TAN) concentration, D) Nitrate concentration. The correlation between AOU [µM] and ΔN₂O [nM] is shown in panel E. Pearson correlation coefficients (r) and their associated p value are shown in each panel.

300

3.4 N₂O Air/Sea and Diapycnal Fluxes

Atmospheric N₂O mole fractions measured at Kinnaook / Cape Grim Air Pollution Station (*see Figure 1*) were observed to increase from 334.7 ppb in July 2022 to 335.9 ppb in February 2023 (*see Error! Reference source not found.*). The April 2023 atmospheric N₂O mole fraction was slightly lower than that observed in February 2023 at 335.6 ppb.

305

Estimated N₂O air/sea flux in the main harbour stations (KR1, C10, C08, WH2) was observed to range from -12.88 (± 0.88) µmol N₂O m⁻² day⁻¹ at C10 in July 2022 (negative sign indicates absorption of N₂O into the surface waters from the atmosphere) to 7.31 (± 0.88) µmol N₂O m⁻² day⁻¹ at the same station in February 2023 (using the “High” K₆₀₀ estimator from **Raymond and Cole (2001)**; *see Table 2*).

310

Station KR1 was always observed to be a net sink for atmospheric N₂O, and every non-endmember station was an estimated sink in July 2022. Near the head of the system, station WH2 was observed to be a net source of



315 N₂O to the atmosphere in October 2022, February 2023, and April 2023, as were stations C10 and C08
(positioned above the deepest basins) in February 2023 and April 2023.

Estimated diapycnal fluxes using local buoyancy frequencies showed a consistent upwards movement of N₂O
from the subhalocline to surface layers with the smallest fluxes observed in July 2022 (49 nmol N₂O m⁻² day⁻¹ at
320 C08) and largest fluxes observed in October 2022 (up to 1308 nmol N₂O m⁻² day⁻¹ at WH2) and February 2023
(up to 1200 nmol N₂O m⁻² day⁻¹ at C10) (**Table 3**). Patterns in the size of the diapycnal flux generally reflected
the patterns of N₂O % saturation with the largest fluxes occurring in October 2022 during the periods of greatest
N₂O % saturation. Overall the magnitude of the estimated diapycnal fluxes was smaller than estimated air/sea
fluxes (smaller) however in February the fluxes were of similar magnitudes.

325

326



327 **Table 2: Estimated sea-to-air N₂O flux (mean $\mu\text{Mol N}_2\text{O m}^{-2} \text{ day}^{-1} \pm$ standard error) of the main harbour stations**
 328 **using calculations presented in Bange et al. (2019) and Zhang et al. (2020) and a range of k_{600} estimators from**
 329 **Raymond and Cole (2001). Low, Mid, and High represent different estimators of k_{600} presented in Raymond and Cole**
 330 **(2001). Positive values indicate the flux of N₂O from the harbour water to the atmosphere. Negative values (shown in**
 331 **with bold text) indicate flux of N₂O from the atmosphere into the harbour water. Estimated Gordon River Flow and**
 332 **Mean (20 day) Gordon Above Dennison (GAD)Stream Gauge are also shown for each month as well as the Pearson**
 333 **Correlation and associated p-values between flow metrics, rainfall, and sea-to-air flux (and surface water %**
 334 **saturation).**

Station	K_{600} Est.	Jul 2022 $\mu\text{mol N}_2\text{O m}^{-2} \text{ day}^{-1}$	Oct 2022 $\mu\text{mol N}_2\text{O m}^{-2} \text{ day}^{-1}$	Feb 2023 $\mu\text{mol N}_2\text{O m}^{-2} \text{ day}^{-1}$	Apr 2023 $\mu\text{mol N}_2\text{O m}^{-2} \text{ day}^{-1}$	Gordon Flow vs Surface Flux	GAD Flow vs Surface Flux	GAD Flow vs % N ₂ O Sat.	Rainfall vs Surface Flux
KR1	High:	-11.07 ± 1.84	-04.01 ± 0.86	-03.30 ± 0.49	-03.17 ± 0.16	r = -0.8316 p = 7.5 x 10 ⁻⁴	r = -0.8624 p = 3.1 x 10 ⁻⁴	r = -0.8726 p = 2.1 x 10 ⁻⁴	r = 0.5577 p = 0.060
	Mid:	-08.45 ± 1.41	-03.19 ± 0.69	-02.55 ± 0.38	-02.44 ± 0.12				
	Low:	-04.69 ± 0.78	-01.93 ± 0.42	-01.46 ± 0.22	-01.38 ± 0.07				
C10	High:	-12.88 ± 0.88	-01.21 ± 1.07	07.31 ± 1.57	02.60 ± 0.85	r = -0.8298 p = 8.4 x 10 ⁻⁴	r = -0.9091 p = 4.2 x 10 ⁻⁵	r = -0.8795 p = 1.6 x 10 ⁻⁴	r = 0.2751 p = 0.387
	Mid:	-09.83 ± 0.67	-00.96 ± 0.85	05.65 ± 1.22	02.00 ± 0.66				
	Low:	-05.46 ± 0.37	-00.58 ± 0.51	03.22 ± 0.69	01.13 ± 0.37				
C08	High:	-03.50 ± 1.82	-01.69 ± 0.38	04.08 ± 1.07	04.57 ± 1.79	r = -0.8547 p = 3.97 x 10 ⁻⁴	r = -0.8804 p = 1.6 x 10 ⁻⁴	r = -0.8447 p = 5.4 x 10 ⁻⁴	r = 0.1846 p = 0.566
	Mid:	-02.67 ± 1.39	-01.34 ± 0.29	03.15 ± 0.83	03.52 ± 1.38				
	Low:	-01.49 ± 0.77	- 0.81 ± 0.18	01.80 ± 0.47	01.98 ± 0.78				
WH2	High:	-10.88 ± 0.68	02.63 ± 0.17	02.40 ± 1.56	03.50 ± 1.72	r = -0.8071 p = 1.51 x 10 ⁻³	r = -0.8269 p = 9.1 x 10 ⁻⁴	r = -0.8077 p = 1.5 x 10 ⁻³	r = 0.6316 p = 0.028
	Mid:	-08.30 ± 0.52	02.09 ± 0.14	01.85 ± 1.20	02.69 ± 1.33				
	Low:	-04.61 ± 0.29	01.26 ± 0.08	01.06 ± 0.69	01.52 ± 0.75				
Gordon River Flow (m ³ sec ⁻¹)		383.6 ± 38.9	360.3 ± 54.1	342.6 ± 74.6	324.3 ± 26.6	-	-	-	-
GAD Flow (m ³ sec ⁻¹)		107.6 ± 15.9	73.7 ± 12.1	38.8 ± 5.1	30.5 ± 2.2	-	-	-	-

335
336

337 **Table 3: Estimated diapycnal N₂O flux (nmol N₂O m⁻² day⁻¹) from 20 m to 2 m within the main harbour stations**
 338 **Positive values indicate the flux of N₂O from the basin water (20 m) to the surface lens (2m).**

Station	July 2022 nmol N ₂ O m ⁻² day ⁻¹	October 2022 nmol N ₂ O m ⁻² day ⁻¹	February 2023 nmol N ₂ O m ⁻² day ⁻¹	April 2023 nmol N ₂ O m ⁻² day ⁻¹
KR1	80	282	992	395
C10	140	1200	1040	454
C08	49	782	778	348
WH2	117	125	1308	240

339
340



341 **4. Discussion**

342 Our study is the first to report on N₂O distribution and air/sea flux from an Australasian fjord-like estuary. We
343 set out to investigate how N₂O concentrations varied along horizontal and depth gradients; how N₂O
344 concentrations and estimated surface water emissions vary seasonally; how N₂O concentrations vary with
345 freshwater inputs; and whether the relationship between AOU and ΔN₂O could help clarify the primary
346 mechanism for N₂O generation in this system.

347

348 We used surface water observations, local wind speed (from Cape Sorell weather station) and atmospheric N₂O
349 mole fractions (from Cape Grimm; **Figure 1**) to estimate N₂O air/sea flux (based on **Zhang et al., (2010)** and
350 **Bange et al., (2019)**) and found that Macquarie Harbour functions as both a sink and a source of N₂O. Most
351 harbour stations were estimated to be a sink for N₂O in July and October 2022 (when river flow was greater) and
352 a source in February and April 2023 (during low river flow periods; *see* **Figure 6** and **Table 2**). Pearson
353 correlations show that when freshwater flow is high N₂O air/sea flux is negative (indicating uptake from the
354 atmosphere) and when freshwater flow is low N₂O air/sea flux is positive (**Table 2**). Our observations highlight
355 that freshwater flow is a key driver of N₂O emissions in this estuary. In addition, Gordon River flow is heavily
356 influenced by hydroelectric dam release (up to ~28% of the flow in July 2023). Rainfall in the catchment area
357 may offset the effects of dam release, but our observations did not capture this as rainfall itself was not
358 significantly correlated with N₂O concentrations or air/sea flux.

359

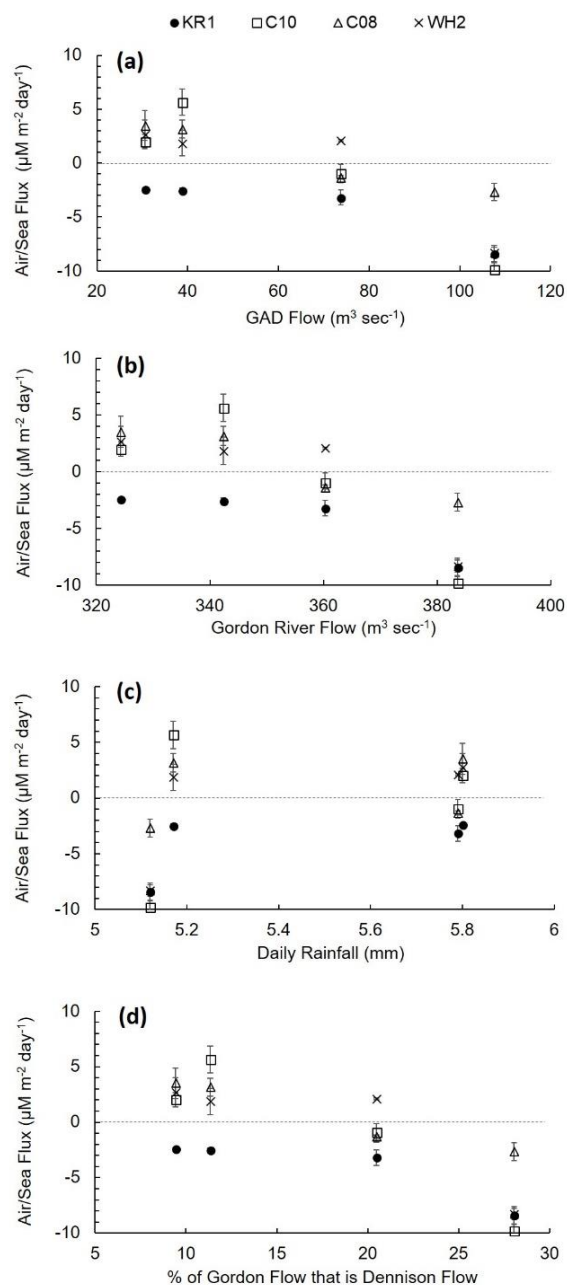
360 The river endmember concentrations of N₂O were often observed to be undersaturated, as observed in the South
361 Platte River Basin, USA, **McMahon and Dennehy 1999**; Neuse River Estuary, USA, **Stow et al., 2005**;
362 headwater streams, Ontario, Canada, **Baulch et al., 2011**; Upper Mara River Basin, Kenya, **Mwanke et al.,**
363 **2019**. Our observations of endmember N₂O concentrations were similar to the lower end of the concentrations
364 reported in **McMahon and Dennehy (1999)** (approx. 80% saturation), but not as low as those reported Jackson
365 Creek, Ontario, Canada in **Baulch et al., (2011)** were some observations reached <20% saturation. N₂O
366 undersaturation in those systems was attributed to complete denitrification (use of N₂O as a terminal electron
367 acceptor by denitrifies) in streams with high DOC loads, low DO, low NO₃⁻ concentrations. It should also be
368 noted that up to 28% of the estimated Gordon River flow was found to be associated with flow through the
369 Gordon Above Dennison stream gauge (a proxy for hydroelectric dam/reservoir release to the Gordon River).
370 Boreal reservoirs have been shown to be net sinks of atmospheric N₂O (**Hendzel et al., 2005**) which was
371 attributed to increased N₂O demand to drive complete denitrification. There is good reason to believe that N₂O
372 may be scavenged in the Gordon and King Rivers as well because they do often have high DOC concentrations,
373 high water column DO demand (**Maxey et al., 2020**), and low DO concentrations in near the stream bed (**Maxey**
374 **et al., 2022**).

375

376 Below the estuary's predominately freshwater surface lens, the fjord-like morphology drives suboxic conditions
377 like those observed in the subhalocline waters at station WH2 in October 2022 (*see* **Figure 3**; **Hartstein et al.,**
378 **2019**; **Maxey et al., 2020, 2022**). While these conditions do not always persist, DO concentrations below 31 μM
379 have been observed to occur more than 30% of the time up estuary, specifically at station WH2 (**Maxey et al.,**
380 **2022**). In layers of the harbour where DO concentrations were lowest (subhalocline layers) we observed the



381 maximum N₂O concentrations (**Figure 4**). Subhalocline N₂O saturation was observed to generally range from
 382 approx. 110% to 170% with the highest values observed within the deeper basins near the foot of the sill
 383 (stations C10 and C08).



384

385 **Figure 6: Mean Air/Sea Flux (µM m⁻² day⁻¹) versus A) Gordon above Dennison River flow (m³ day⁻¹), B) estimated**
 386 **Gordon River flow (m³ day⁻¹), C) daily rainfall (mm) (20 day mean), and D) % of estimated Gordon River flow this is**
 387 **accounted for by the Gordon above Dennison River gauge (proxy for hydroelectric dam release). Error bars indicate**
 388 **± 1 standard error.**



389 In the harbour's subhalocline layer there is not enough light to support photosynthesis (**Hartstein et al., 2019;**
390 **Maxey et al., 2017, 2020, and 2022**) and thus the main source of oxygen is advection from marine intrusions.
391 N₂O producing microbes have been observed to populate this layer of the harbour (*see Da Silva et al., 2021 and*
392 **2022**) and our observations of supersaturated N₂O in these layers show that those microbes are active. The linear
393 relationship between AOU and ΔN_2O (slope = 0.0154; $r = 0.596$; $p = 2.4 \times 10^{-23}$; **Figure 5C**) indicates that N₂O
394 production occurs primarily through the ammonia oxidation (nitrification) pathway (**Yoshinari, 1976; Walter et**
395 **al., 2004; Brase et al., 2017**). Our observations are on the lower end of the range reported nitrification slopes
396 (see **Suntharalingam and Sarmiento, 2000; Brase et al., 2017**) indicating a low yield of N₂O per mole O₂
397 consumed. These more modest yields are likely an artefact of mixing and loss dynamics such as basin water DO
398 recharges from marine intrusions, and loss to aerobic respiration and loss to the atmosphere. This suggests that
399 some portion of subhalocline pelagic oxygen demand in the harbour can be attributed to nitrifying microbes
400 (albeit at a much lower rate compared to aerobic respiration). **Ji et al., (2020)** also observed similar relationships
401 in the Saanich Inlet, a seasonally anoxic fjord-like estuary in British Columbia, but in that system anoxic
402 conditions are more persistent (**Bourbonnais et al., 2013; Manning et al., 2010**) compared to Macquarie
403 Harbour (**Maxey et al., 2022**). Deep-water renewal / marine intrusions have been hypothesized to stimulate N₂O
404 production in the Saanich Inlet (**Capelle et al., 2018; Michiles et al., 2019; Ji et al., 2020**), and Baltic Sea
405 (**Walter et al., 2006**) and may also be stimulating it in Macquarie Harbour as well. In the Baltic Sea, **Walter et**
406 **al. (2006)** and **Mylykangas et al. (2017)** observed enhanced N₂O production in areas receiving significant
407 marine intrusions. Positive correlations between AOU and ΔN_2O observed in western Baltic Sea waters (**Walter**
408 **et al., 2006**) along with mean (11-year; 2006-2017) seasonal variations in DO and N₂O observed through the
409 water column at the Boknis Eck Time-Series Station (Eckernförde Bay, Southwest Baltic Sea) indicate a tight
410 coupling between DO supply and N₂O production (presumably by nitrification) / consumption (presumably by
411 denitrification) pathways in that area (**Ma et al., 2019**). The reintroduction of marine water on the upstream side
412 of a dam in the Nakong River, South Korea was found to affect bottom water trapping (stagnation), DO
413 conditions, N process rates, process specific gene abundances, and subsequently the fate of N in that system
414 (**Huang et al., 2024**). Marine intrusions primarily refresh the DO supply adjacent to the sill in Macquarie
415 Harbour (near station C10) and since we also observed a positive correlation between AOU and ΔN_2O they offer
416 a possible explanation for the higher subhalocline N₂O concentrations observed there.

417

418 We conceptualize that during periods of high river flow, the surface water lens thickens and transports water
419 undersaturated with N₂O quickly across the harbour surface and out of Hells Gates inlet. Some N₂O from the
420 oversaturated subhalocline water is entrained in the surface lens (diapycnal flux) and transported out of the
421 system in its dissolved form. During periods of low river flow, the surface lens is thinner and residence times
422 longer (**Andrewartha and Wild-Allen 2017; Maxey et al., 2022**). N₂O from the oversaturated subhalocline
423 water then diffuses through the surface layer and escapes into the atmosphere in its gaseous form (**Figure 7**). Our
424 estimates of diapycnal flux indicate that the mass transport from subhalocline waters is smaller (~2x smaller)
425 than the air/sea flux supporting this idea. This conceptual model suggests that the harbour surface lens functions
426 as a sink for both atmospheric N₂O and N₂O generated in the subhalocline layer during high flow periods
427 (**Figure 7**).

428



429 Previous work in Australian estuaries with pristine catchments (like Macquarie Harbour) has shown that many
430 tend to function as a sink for atmospheric N₂O (Maher *et al.*, 2016; Wells *et al.*, 2018). Our study adds the
431 caveat that source sink dynamics may also depend on factors controlling river flow in deeper stratified systems.
432 Despite the advancements made to date, many of the deeper estuaries in Chile, Australia and New Zealand are
433 lacking descriptions of N₂O source sink dynamics (*e.g.* Bathurst Harbour, Tasmania; fjords of South Island New
434 Zealand; estuaries on Stewart Island New Zealand). Given that these systems have relatively pristine catchments
435 they offer an opportunity to better understand natural fjord-like estuarine responses to the climate drivers of N₂O
436 dynamics. Mesoscale climate oscillations (*i.e.* the Southern Annular Mode; SAM; North Atlantic Oscillation;
437 NAO) have been shown to affect rainfall, river flow, and dissolved oxygen concentrations in this and other fjord-
438 like estuaries (Maxey *et al.*, 2022; Austin and Inall, 2002). In Western Tasmania, SAM in its positive phase
439 results in increased orographic rainfall and a greater propensity for higher river flow, possibly tilting the source
440 and sink balance to net N₂O uptake during these periods.

441

442 Climate change predictions for Tasmania's West Coast (which includes the Macquarie Harbour catchment)
443 indicate that the region will experience a more extreme precipitation regime with increased winter precipitation
444 and decreased summer precipitation (Grose *et al.*, 2010; Bennett *et al.*, 2010). If these future predictions result
445 in more extreme seasonality in Gordon River flow, then the harbour may respond in kind with a larger variation
446 in N₂O source and sink dynamics *i.e.* larger N₂O sink in winter and N₂O source in summer. However, given that
447 the river flow is somewhat regulated by the hydroelectric dam, our study suggests that flow regulation has the
448 potential to augment harbour N₂O emissions. Releasing water during extreme low rainfall periods might allow
449 N₂O slowly accumulating in subhalocline waters to be released in the exported surface lens.

450

451 It is well established that fjord and fjord-like estuaries are important sites of C burial (Smith *et al.*, 2015;
452 Bianchi *et al.*, 2018, 2020). This study supports the idea that they can also be important sites of N₂O
453 sequestration. Macquarie Harbour air/sea flux estimates are similar in magnitude to observations made in other
454 stratified estuaries and enclosed seas such as the Reloncaví Estuary, Chile (Yevenes *et al.*, 2017) and
455 Eckernförde Bay, Germany (Ma *et al.*, 2019) (Table A1). Macquarie Harbour, however, was observed to have
456 lower fluxes of N₂O into the atmosphere than other river dominated, but not fjord-like, estuaries (Elbe River,
457 Germany; Schulz *et al.*, 2023) including those on the Australian mainland's east coast (Wells *et al.*, 2018).

458

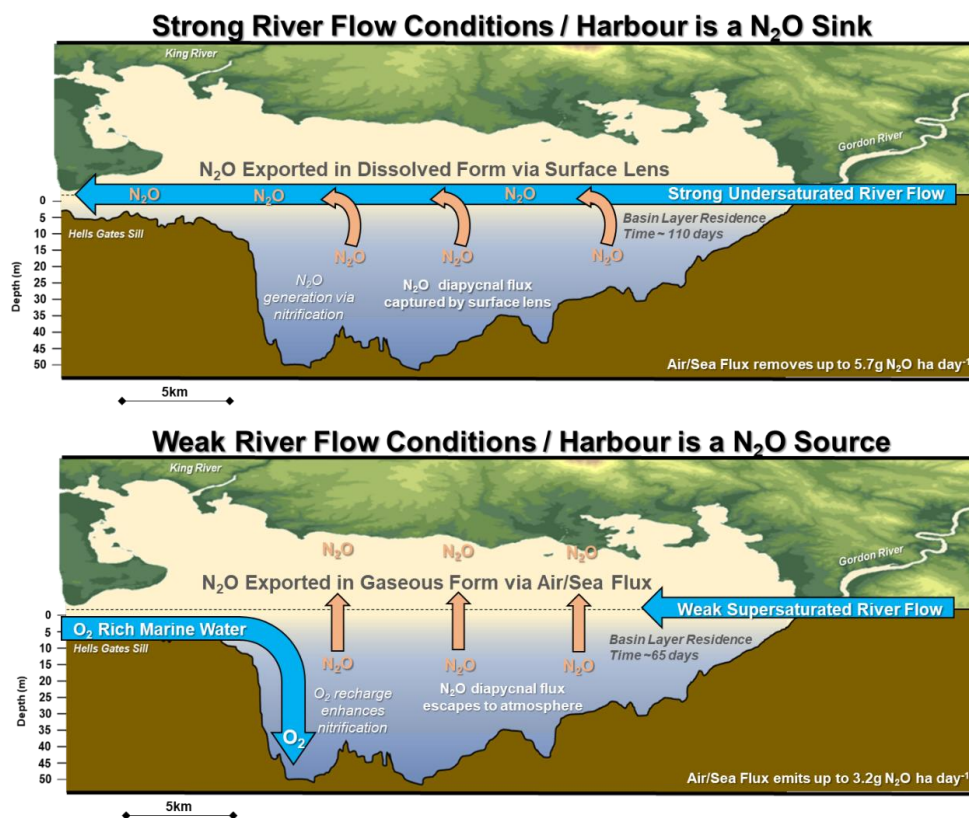
459 Fjord and fjord-like estuaries are defined by their strong stratification and sensitivity to freshwater inputs. With
460 climate change, rainfall patterns are expected to become more extreme and thus alter the river flow, and
461 subsequently N₂O source sink dynamics in these systems on a global scale. In systems that are expected to
462 experience increasingly drier conditions they may shift from net sinks of N₂O to sources, and further perpetuate
463 the accumulation of N₂O in the atmosphere.

464 5. Conclusions

465 In summary, river flow, and specifically river flow driven by hydroelectric dam release, significantly affects both
466 surface water N₂O concentrations and air/sea flux in Macquarie Harbour. Importantly, when river flow is low



467 most of the harbour emits N_2O to the atmosphere. When river flow is high most of the harbour removes N_2O
 468 from the atmosphere and intercepts the diapycnal flux exporting N_2O to the ocean in its dissolved form.
 469
 470 N_2O is continually supersaturated below the halocline and the relationship between AOU and ΔN_2O indicate that
 471 the main N_2O generation process is nitrification. Climate change is predicted to result in wetter winter / drier
 472 summers for the Tasmanian West Coast, which may result in augmented N_2O air/sea fluxes.
 473
 474 These represent the first descriptions of N_2O spatiotemporal distribution, estimated air/sea flux, estimated
 475 diapycnal flux, and N_2O production pathways in this system.
 476



477
 478 **Figure 7: Conceptual model of Macquarie Harbour's N_2O dynamics.** The top diagram depicts the capture of N_2O
 479 generated in the subhalocline during strong river flow conditions. Here N_2O is exported from the harbour in its
 480 dissolved form via undersaturated surface flows from the harbour to the ocean. The bottom diagram depicts the
 481 efflux of N_2O from the harbour surface during low flow conditions. Note that during these conditions the surface
 482 flows are weak and generally supersaturated with N_2O permitting its escape in gaseous form to the atmosphere.

483



484 **6. Appendix**

485 **Table A1: N₂O fluxes and observed ranges of mean (± standard deviation) N₂O concentration / saturation from both**
 486 **fjord-like / river dominated estuaries around the globe and estuaries in Australia.**

Location	System Type	Measurement Depth Range	Mean Sea-to-Air N ₂ O flux uMol N ₂ O m ⁻² day ⁻¹	Min and Max Sea-to-Air N ₂ O flux uMol N ₂ O m ⁻² day ⁻¹	Mean N ₂ O Concentration (and Saturation) nM N ₂ O (and %)	Min and Max N ₂ O Concentration (and Saturation) nM N ₂ O (and %)	Reference
Macquarie Harbour, Western Tasmania, Australia	Fjord-like Estuary	2m to 45m	-09.83 ± 0.67 to 05.65 ± 1.22	-10.82 to 7.73	11.7 ± 1.6 (121.8 ± 17.8)	7.87 to 17.12 (81 to 174)	<i>This Study</i>
Reloncaví Estuary, Chile	Fjord-like Estuary	0m to 5m	0.86 ± 2.28	-1.58 to 5.60	11.8 ± 1.70 (111 ± 18.3)	8.34 to 14.5 (80 to 140)	Yevenes <i>et al.</i> , 2017
Reloncaví Estuary, Chile	Fjord-like Estuary	10m to 200m	-	-	14.5 ± 1.73 (145 ± 17.7)	10.5 to 17.0 (11 to 170)	Yevenes <i>et al.</i> , 2017
Chiloé Interior Sea, Chile	Fjord-like Estuary	0m to 200m	1.08 ± 1.41	-0.18 to 3.19	12.6 ± 2.36 (121 ± 17.5)	8.81 to 21.1 (87 to 160)	Yevenes <i>et al.</i> , 2017
Europa Sound, Magellanic Region, Chile	Fjord-like Estuary	1m to 10m	-15.22 to -0.81	-	11.9 ± 5.7 to 12.7 ± 1.0	-	Fariás <i>et al.</i> , 2018
Concepción Channel, Magellanic Region, Chile	Fjord-like Estuary	1m to 150m	0.69 to 7.70	-	13.6 ± 1.1 to 17.0 ± 0.02	-	Fariás <i>et al.</i> , 2018
Sarmiento Channel, Magellanic Region, Chile	Fjord-like Estuary	1m to 10m	2.07 to 12.53	-	13.1 ± 0.1 to 16.5 ± 0.3	-	Fariás <i>et al.</i> , 2018
Estero Peel, Magellanic Region, Chile	Fjord-like Estuary	1m to 10m	0.11 to 2.01	-	13.1 ± 0.2 to 13.5 ± 0.5	-	Fariás <i>et al.</i> , 2018
Estero Calvo, Magellanic Region, Chile	Fjord-like Estuary	1m to 10m	0.04	-	13.9 ± 0.8	-	Fariás <i>et al.</i> , 2018
Estero Amalia, Magellanic Region, Chile	Fjord-like Estuary	1m to 100m	-0.08	-	14.2 ± 1.7	-	Fariás <i>et al.</i> , 2018
Estero las Montañas, Magellanic Region, Chile	Fjord-like Estuary	1m to 10m	-2.95	-	9.69 ± 1.6	-	Fariás <i>et al.</i> , 2018
Smyth Channel, Magellanic Region, Chile	Fjord-like Estuary	1m to 300m	1.07 to 11.2	-	14.3 ± 0.4 to 16.0 ± 0.5	-	Fariás <i>et al.</i> , 2018
Última Esperanza Sound, Magellanic Region, Chile	Fjord-like Estuary	1m to 10m	-3.7 to 10.4	-	12.1 ± 1.1 to 13.7 ± 0.07	-	Fariás <i>et al.</i> , 2018
Almirante Montt Gulf, Magellanic Region, Chile	Fjord-like Estuary	1m to 150m	15.6	-	21.0 ± 5.7	-	Fariás <i>et al.</i> , 2018
Kirke Channel, Magellanic Region, Chile	Fjord-like Estuary	1m to 10m	0.12 to 8.19	-	13.3 ± 0.1 to 15.4 ± 0.4	-	Fariás <i>et al.</i> , 2018
Union Channel, Magellanic Region, Chile	Fjord-like Estuary	1m to 10m	22.1	-	16.7 ± 0.8	-	Fariás <i>et al.</i> , 2018
Union Sound, Magellanic Region, Chile	Fjord-like Estuary	1m to 10m	2.86	-	14.8 ± 0.8	-	Fariás <i>et al.</i> , 2018
Western Magellan Strait, Magellanic Region, Chile	Fjord-like Estuary	1m to 10m	143	-	15.71	-	Fariás <i>et al.</i> , 2018
Eastern Magellan Strait, Magellanic Region, Chile	Fjord-like Estuary	1m	36.3	-	16.4	-	Fariás <i>et al.</i> , 2018
San Gregorio Cape, Magellanic Region, Chile	Fjord-like Estuary	1m	24.8	-	12.07	-	Fariás <i>et al.</i> , 2018
Otway Center Sound, Magellanic Region, Chile	Fjord-like Estuary	1m	35.5	-	11.4	-	Fariás <i>et al.</i> , 2018
Magdalena North Channel, Magellanic Region, Chile	Fjord-like Estuary	1m	-0.22	-	11.4	-	Fariás <i>et al.</i> , 2018
Chasco Sound, Magellanic Region, Chile	Fjord-like Estuary	1m	6.81	-	16.01	-	Fariás <i>et al.</i> , 2018
Cockburn West Channel, Magellanic Region, Chile	Fjord-like Estuary	1m	6.18	-	14.47	-	Fariás <i>et al.</i> , 2018
Saanich Inlet, British Columbia, Canada	Fjord-like Estuary	10m to 200m	2.3 ± 2.5 to 3.9 ± 2.9	-	14.7	<0.5 to 37.4	Capelle <i>et al.</i> , 2018
Saanich Inlet, British Columbia, Canada	Fjord-like Estuary	Surface to 110m	11.3 to 20.4	-	-	-	Cohen 1978
Elbe River Estuary, Germany	Well-Mixed River Dominated Estuary	1.2m	-	26.0 ± 23.5 to 100.7 ± 101.2	-	(161 ± 53.6) to (243 ± 141.6)	Schulz <i>et al.</i> 2023
Eckernförde Bay, Boknis Eck Time Series Station, Baltic Sea, Germany	Enclosed Sea	1m to 25m	3.5 ± 12.4	-19.0 to 105.7	(111 ± 30)	(56 to 314)	Ma <i>et al.</i> , 2019
Eckernförde Bay, Boknis Eck Time Series Station, Baltic Sea, Germany	Enclosed Sea	1m to 25m	-	-	10 to 17	-	Walter <i>et al.</i> , 2006
Baltic Sea, Germany	Enclosed Sea	110m	5 -11	-	14 to 1523	-	Römer 1983



Gotland Basin, Baltic Sea, Germany	Enclosed Sea	90m	-	-	13	0 to 126 (0 to 450)	Brettar and Rheinheimer 1991
Northwest Shelf, Black Sea	Enclosed Sea	-	1.6 to 4.4	-	6.5 to 8	-	Amouroux <i>et al.</i> , 2002
Deep Basin, Black Sea	Enclosed Sea	70m	3.1 to 5.2	-	7.5 to 10.2	-	Amouroux <i>et al.</i> , 2002
Cariaco Basin, Venezuela	Coastal Basin	Surface to 400m	-	-	4.4 to 5.5	-	Hashimoto <i>et al.</i> , 1983
Guadalquivir Estuary, Gulf of Cadiz, Spain	River Dominated Estuary	2m	18.7 ± 33.6	-	20.6 ± 24.3	-	Sierra <i>et al.</i> , 2020
Guadalquivir Estuary, Gulf of Cadiz, Spain	River Dominated Estuary	2m	0.3 ± 0.5	-	6.7 ± 0.4	-	Sierra <i>et al.</i> , 2020
Guadalquivir Estuary, Gulf of Cadiz, Spain	River Dominated Estuary	2m	0.9 ± 21.6	-	7.3 ± 15.4	-	Sierra <i>et al.</i> , 2020
Noosa River Estuary, Eastern Australia	River Dominated Estuary	0.5m to 9.6m	-14.24 ± 14.02	-57.72 to 22.20	6.99 ± 0.43 (97 ± 2.2)	5.92 to 7.95 (90 to 103)	Wells <i>et al.</i> , 2018
Mooloolah River Estuary, Eastern Australia	River Dominated Estuary	0.5m to 6.8m	-7.33 ± 7.25	-48.76 to 16.31	6.74 ± 0.64 (97 ± 3.8)	5.19 to 7.71 (82 to 112)	Wells <i>et al.</i> , 2018
Maroochy River Estuary, Eastern Australia	River Dominated Estuary	0.5m to 8.2m	51.33 ± 55.3	-34.94 to 179.64	8.4 ± 1.50 (113 ± 16.7)	6.07 to 12.93 (92 to 163)	Wells <i>et al.</i> , 2018
Pine River Estuary, Eastern Australia	River Dominated Estuary	0.5m to 10.1m	17.10 ± 39.44	-33.22 to 145.50	7.1 ± 0.76 (102 ± 6.24)	6.05 to 8.57 (93 to 117)	Wells <i>et al.</i> , 2018
Brisbane River Estuary, Eastern Australia	River Dominated Estuary	0.5m to 23.9m	209.54 ± 143.59	15.42 to 662.62	9.8 ± 1.36 (133 ± 9.9)	6.75 to 12.75 (105 to 158)	Wells <i>et al.</i> , 2018
Middle Reach, Brisbane River Estuary, Eastern Australia	River Dominated Estuary	Surface	14.5 ± 1.19	5.4 ± 0.34 to 25.2 ± 1.87	-	13.1 to 17.9 (160 to 250)	Sturm <i>et al.</i> , 2017
Lower Reach, Brisbane River Estuary, Eastern Australia	River Dominated Estuary	Surface	6 ± 0.51	3.7 ± 0.85 to 9.1 ± 1.19	-	9.2 to 12.7 (125 to 410)	Sturm <i>et al.</i> , 2017
Oxley Creek, Eastern Australia	River Dominated Estuary	2.1m to 13.1m	210.59 ± 60.23	91.54 to 280.16	11.7 ± 1.34 (156 ± 19.7)	9.65 to 14.89 (139 to 199.7)	Wells <i>et al.</i> , 2017
Nerang River Estuary, Eastern Australia	River Dominated Estuary	0.5m to 6.8m	-0.62 ± 20.87	-67.98 to 45.92	6.73 ± 0.43 (100 ± 4.3)	5.99 to 7.79 (88 to 109)	Wells <i>et al.</i> , 2018
Logan River Estuary, Eastern Australia	-	0.5m to 14.4m	110.00 ± 153.55	-54.48 to 796.00	9.3 ± 2.36 (127 ± 27.5)	5.54 to 14.8 (81 to 191)	Wells <i>et al.</i> , 2018
Albert River Estuary, Eastern Australia	-	1.1m to 15.7m	90.05 ± 73.32	-9.50 to 264.25	10.10 ± 2.24 (131 ± 29.8)	7.32 to 15.1 (98 to 205)	Wells <i>et al.</i> , 2018
Darwin Creek, Australia	Mangrove Creek	~1m	-0.12	-	6.3 (98.9)	6.0 to 6.8 (95 to 104)	Maher <i>et al.</i> , 2016
Hinchinbrook Creek, Australia	Mangrove Creek	~1m	-3.43	-	6.1 (83.3)	5.6 to 6.8 (75 to 91)	Maher <i>et al.</i> , 2016
Melbourne Creek, Australia	Mangrove Creek	~1m	-1.33	-	7.9 (96.6)	6.9 to 9.1 (86 to 115)	Maher <i>et al.</i> , 2016
Morton Bay Creek, Australia	Mangrove Creek	~1m	-3.19	-	5.1 (77.4)	3.4 to 6.6 (50 to 105)	Maher <i>et al.</i> , 2016
Seventeen Seventy Creek, Australia	Mangrove Creek	~1m	-1.75	-	7.7 (94.3)	7.1 to 8.9 (88 to 106)	Maher <i>et al.</i> , 2016
Brisbane River, Australia	-	-	-	-	(285)	(135 to 435)	Musenze <i>et al.</i> , 2014
Coffs Creek, Australia	-	-	-	-	(219 ± 37)	(53 to 386)	Reading <i>et al.</i> , 2017
Coffs Creek, Australia	-	-	-	-	(266.5 ± 128)	(86 to 678)	Reading <i>et al.</i> , 2020
Boambee Creek, Australia	-	-	-	-	(197.1 ± 75)	(87 to 329)	Reading <i>et al.</i> , 2020
Bonville Creek, Australia	-	-	-	-	(183.7 ± 65)	(78 to 310)	Reading <i>et al.</i> , 2020
Pine Creek, Australia	-	-	-	-	(194.1 ± 65)	(79 to 382)	Reading <i>et al.</i> , 2020
Yarra River, Australia	Salt Wedge Estuary	-	-	-	(135.9 ± 31)	-	Tait <i>et al.</i> , 2017



487 **7. Acknowledgments**

488 We would like to thank GEOMAR for providing the facilities and training (thank you Lea, Florian, and
489 Chukwudi) required to analyse N₂O samples. We want to thank Torsten and Leonie Schwoch for their sampling
490 assistance and tireless vessel operation on the Harbour. We want to thank the ADS Environmental Services *Sdn.*
491 *Bhd.* technical staff for helping to collect portions of this dataset (Grace, Shukry, Atika, Chance, Gene, and
492 Azza). We would also like to thank our families for supporting our long days away from home.

493

494 This research has been supported by internal funding from ADS Environmental Services, Swinburne University
495 of Technology student travel grant, and GEOMAR.

496

497 We have used some of the data available in the MEMENTO database. The MEMENTO database is administered
498 by the Kiel Data Management Team at GEOMAR Helmholtz Centre for Ocean Research Kiel. The database is
499 accessible through the MEMENTO webpage: <https://memento.geomar.de>.



500 **8. Data Availability**

501 This data set is available upon request

502 **9. Author Contributions**

503 **Johnathan Daniel Maxey** – *Conceptualization, Field Collection, Analytical Methodology, Data*
504 *Analysis, Writing – Original Draft, Writing – Review & Editing*

505

506 **Neil David Hartstein** – *Conceptualization, Field Collection, Analytical Guidance, Writing – Review &*
507 *Editing, Funding*

508

509 **Hermann W. Bange** – *Conceptualization, Analytical Methodology, Data Analysis, Writing – Review*
510 *& Editing*

511

512 **Moritz Müller** – *Conceptualization, Field Collection, Analytical Guidance, Writing – Review &*
513 *Editing*

514

515 **10. Competing Interests**

516 HWB serves on the editorial board for Biogeosciences. The authors declare that they have no other conflicts of
517 interest.

518

519 **11. References**

520 Borges, A. V., Delille, B., Schiettecatte, L. S., Gazeau, F., Abril, G., and Frankignoulle, M.: Gas transfer
521 velocities of CO₂ in three European estuaries (Randers Fjord, Scheldt, and Thames). *Limnology and*
522 *Oceanography*, 49(5), 1630-1641, 2004. DOI: 10.4319/lo.2004.49.5.1630

523

524 Acuña-González, J. A., Vargas-Zamora, J. A., and Córdoba-Muñoz, R.: A snapshot view of some vertical
525 distributions of water parameters at a deep (200 m) station in the fjord-like Golfo Dulce, embayment, Costa Rica.
526 *Revista de Biología Tropical*, 54(1), 193-200, 2006. ISSN: 0034-7744

527

528 Amouroux, D., Roberts, G., Rapsomanikis, S., and Andreae, M. O.: Biogenic gas (CH₄, N₂O, DMS) emission to
529 the atmosphere from near-shore and shelf waters of the north-western Black Sea. *Estuarine, Coastal and Shelf*
530 *Science*, 54(3), 575-587, 2002. DOI: 10.1006/ecss.2000.0666

531



- 532 Andrewartha, J. and Wild-Allen, K.: CSIRO Macquarie Harbour Hydrodynamic and Oxygen Tracer Modelling.
533 Progress report to FRDC 2016/067 Project Steering Committee, 2017.
534
- 535 Arneborg, L., Janzen, C., Liljebladh, B., Rippeth, T. P., Simpson, J. H., and Stigebrandt, A.: Spatial variability of
536 diapycnal mixing and turbulent dissipation rates in a stagnant fjord basin. *Journal of Physical Oceanography*,
537 34(7), 1679-1691, 2004. DOI: 10.1175/1520-0485(2004)034<1679:SVODMA>2.0.CO;2
538
- 539 Austin, W. E., and Inall, M. E.: Deep-water renewal in a Scottish fjord: temperature, salinity and oxygen
540 isotopes. *Polar Research*, 21(2), 251-257, 2002. DOI: 10.3402/polar.v21i2.6485
541
- 542 Bange, H. W., Rapsomanikis, S., and Andreae, M. O.: Nitrous oxide in coastal waters. *Global Biogeochemical*
543 *Cycles*, 10(1), 197-207, 1996. DOI: 10.1029/95GB03834.
544
- 545 Bange, H. W.: Nitrous oxide and methane in European coastal waters. *Estuarine, Coastal and Shelf Science*,
546 70(3), 361-374, 2006. DOI: 10.1016/j.ecss.2006.05.042
547
- 548 Bange, H. W., Bell, T. G., Cornejo, M., Freing, A., Uher, G., Upstill-Goddard, R. C., and Zhang, G. L.:
549 MEMENTO: A proposal to develop a database of marine nitrous oxide and methane measurements.
550 *Environmental Chemistry*, 6, 195-197, 2009. DOI: 10.1071/en09033.
551
- 552 Bange, H. W., Sim, C. H., Bastian, D., Kallert, J., Kock, A., Mujahid, A., and Müller, M.: Nitrous oxide (N₂O)
553 and methane (CH₄) in rivers and estuaries of northwestern Borneo. *Biogeosciences*, 16(22), 4321-4335, 2019.
554 DOI: 10.5194/bg-16-4321-2019
555
- 556 Bange, H. W., Mongwe, P., Shutler, J. D., Arévalo-Martínez, D. L., Bianchi, D., Lauvset, S. K., Liu, C., Löscher,
557 C. R., Martins, H., Rosentreter, J. A., Schmale, O., Steinhoff, T., Upstill-Goddard, R. C., Wanninkhof, R.,
558 Wilson, S. T., and Xie, H.: Advances in understanding of air–sea exchange and cycling of greenhouse gases in
559 the upper ocean, *Elementa: Science of the Anthropocene*, 12, 2024. DOI: 10.1525/elementa.2023.00044
560
- 561 Bastian, D.: N₂O und CH₄ Verteilung in Ästuaren und Flüssen im Nordwesten von Borneo, 2017. BSc thesis,
562 Kiel University, Kiel, 50 pp., 2017.
563
- 564 Baulch, H. M., Schiff, S. L., Maranger, R., and Dillon, P. J.: Nitrogen enrichment and the emission of nitrous
565 oxide from streams. *Global Biogeochemical Cycles*, 25(4), 2011. DOI: 10.1029/2011GB004047
566
- 567 Beaulieu, J. J., Shuster, W. D., and Rebholz, J. A.: Controls on gas transfer velocities in a large river. *Journal of*
568 *Geophysical Research: Biogeosciences*, 117(G2), 2012. DOI: 10.1029/2011JG001794
569
- 570 Bennett, J. C., Ling, F. L. N., Graham, B., Grose, M. R., Corney, S. P., White, C. J., Holz, G. K., Post, D. A.,
571 Gaynor, S. M. and Bindoff, N. L.: Climate Futures for Tasmania: water and catchments technical report.



- 572 Antarctic Climate & Ecosystems Cooperative Research Centre, Hobart, Tasmania, 2010. ISBN: 978-1-921197-
573 06-8
574
- 575 Bianchi, T. S., Cui, X., Blair, N. E., Burdige, D. J., Eglinton, T. I., and Galy, V.: Centers of organic carbon burial
576 and oxidation at the land-ocean interface. *Organic Geochemistry*, 115, 138-155, 2018. DOI:
577 10.1016/j.orggeochem.2017.09.008
578
- 579 Bianchi, T. S., Arndt, S., Austin, W. E., Benn, D. I., Bertrand, S., Cui, X., Faust, J., Kozirowska-Makuch, K.,
580 Moy, C., Savage, C., Smeaton, C., Smith, R., and Syvitski, J.: Fjords as aquatic critical zones (ACZs). *Earth-
581 Science Reviews*, 203(103145), 2020. DOI: 10.1016/j.earscirev.2020.103145
582
- 583 Brase, L., Bange, H. W., Lendt, R., Sanders, T., and Dähnke, K.: High resolution measurements of nitrous oxide
584 (N_2O) in the Elbe estuary. *Frontiers in Marine Science*, 4(162), 2017. DOI: 10.3389/fmars.2017.00162
585
- 586 Breider, F., Yoshikawa, C., Makabe, A., Toyoda, S., Wakita, M., Matsui, Y., Kawagucci, S., Fujiki, T., Harada,
587 N. and Yoshida, N.: Response of N_2O production rate to ocean acidification in the western North Pacific. *Nature
588 Climate Change*, 9(12), 954-958, 2019. DOI: 10.1038/s41558-019-0605-7
589
- 590 Breitburg, D., Grégoire, M., and Isensee, K. (eds): Global Ocean Oxygen Network 2018. The ocean is losing its
591 breath: Declining oxygen in the world's ocean and coastal waters. OC-UNESCO, IOC Technical Series, No. 137,
592 2018.
593
- 594 Brettar, I., and Rheinheimer, G.: Denitrification in the Central Baltic: evidence for H_2S -oxidation as motor of
595 denitrification at the oxic-anoxic interface. *Marine Ecology Progress Series*, 77(2-3), 157-169, 1991.
596 <http://www.jstor.org/stable/24826569>
597
- 598 Bourbonnais, A., Lehmann, M. F., Hamme, R. C., Manning, C. C., and Juniper, S. K.: Nitrate elimination and
599 regeneration as evidenced by dissolved inorganic nitrogen isotopes in Saanich Inlet, a seasonally anoxic fjord.
600 *Marine Chemistry*, 157, 194–207, 2013. DOI: 10.1016/j.marchem.2013.09.006
601
- 602 Capelle, D. W., Hawley, A. K., Hallam, S. J., and Tortell, P. D.: A multi-year time-series of N_2O dynamics in a
603 seasonally anoxic fjord: Saanich Inlet, British Columbia. *Limnology and Oceanography*, 63(2), 524-539, 2018.
604 DOI: 10.1002/lno.10645
605
- 606 Carpenter, P. D., Butler, E. C. V., Higgins, H. W., Mackey, D. J., and Nichols, P. D.: Chemistry of trace
607 elements, humic substances and sedimentary organic matter in Macquarie Harbour, Tasmania. *Marine and
608 Freshwater Research*, 42(6), 625-654, 1991. DOI: 10.1071/MF9910625
609



- 610 Chen, C., Pan, J., Xiao, S., Wang, J., Gong, X., Yin, G., Hou, L., Liu, M., and Zheng, Y.: Microplastics alter
611 nitrous oxide production and pathways through affecting microbiome in estuarine sediments. *Water Research*
612 221(118733), 2022. DOI: 10.1016/j.watres.2022.118733
613
- 614 Chen, J., Wells, N. S., Erler, D. V., and Eyre, B. D.: Land-use intensity increases benthic N₂O emissions across
615 three sub-tropical estuaries. *Journal of Geophysical Research: Biogeosciences* 127, 2022. DOI:
616 10.1029/2022JG006899
617
- 618 Cresswell, G. R., Edwards, R. J., Barker, B. A.: Macquarie Harbour, Tasmania-seasonal oceanographic
619 surveys in 1985. *University of Tasmania Journal contribution*. 1989. DOI: 10.26749/rstpp.123.63
620
- 621 de Bie, M. J. M.: Factors controlling nitrification and nitrous oxide production in the Schelde estuary. Doctoral
622 dissertation, Yerseke: Netherlands Institute of Ecology (NIOO-CEMO). 2002.
623
- 624 Dey, R., Lewis, S. C., Arblaster, J. M., and Abram, N. J.: A review of past and projected changes in Australia's
625 rainfall. *Wiley Interdisciplinary Reviews: Climate Change*, 10(3), e577, 2019. DOI: 10.1002/wcc.577
626
- 627 Etminan, M., Myhre, G., Highwood, E. J., and Shine, K. P.: Radiative forcing of carbon dioxide, methane, and
628 nitrous oxide: A significant revision of the methane radiative forcing. *Geophysical Research Letters*, 43(24), 12-
629 614, 2016. DOI: 10.1002/2016GL071930
630
- 631 Eyring, V., Gillett, N. P., Achuta Rao, K. M., Barimalala, R., Barreiro Parrillo, M., Bellouin, N., Cassou, C.,
632 Durack, P. J., Kosaka, Y., McGregor, S., Min, S., Morgenstern, O., Sun, Y.: Human Influence on the Climate
633 System. In *Climate Change 2021: The Physical Science Basis. Contribution of Working Group I to the Sixth*
634 *Assessment Report of the Intergovernmental Panel on Climate Change*. Masson-Delmotte, V., Zhai, P., Pirani,
635 A., Connors, S. L., Péan, C., Berger, S., Caud, N., Chen, Y., Goldfarb, L., Gomis, M. I., Huang, M., Leitzell,
636 K., Lonnoy, E., Matthews, J. B. R., Maycock, T. K., Waterfield, T., Yelekçi, O., Yu, R., and Zhou, B. (eds.):
637 Cambridge University Press, Cambridge, United Kingdom and New York, NY, USA, 423–552, 2021. DOI:
638 10.1017/9781009157896.005.
639
- 640 Fariás, L., Bello, E., Arancibia, G., Fernandez, J.: Distribution of dissolved methane and nitrous oxide in Chilean
641 coastal systems of the Magellanic Sub-Antarctic region (50°– 55°S). *Estuarine, Coastal and Shelf Science*, 215,
642 225-240, 2018. DOI: 10.1016/j.ecss.2018.10.020.
643
- 644 Fer, I.: Scaling turbulent dissipation in an Arctic fjord. *Deep Sea Research Part II: Topical Studies in*
645 *Oceanography*, 53(1-2), 77-95, 2006. DOI: 10.1016/j.dsr2.2006.01.003
646
- 647 Forster P., Storelvmo T., Armour K., Collins W., Dufresne J.-L., Frame D., Lunt, D., Mauritsen, T., Palmer, M.,
648 Watanabe, M., Wild, M.: The earth's energy budget, climate feedbacks, and climate sensitivity In *Climate*
649 *Change 2021: The Physical Science Basis. Contribution of Working Group I to the Sixth Assessment Report of*



- 650 the Intergovernmental Panel on Climate Change. Masson-Delmotte, V., Zhai, P., Pirani, A., Connors, S. L.,
651 Péan, C., Berger, S., Caud, N., Chen, Y., Goldfarb, L., Gomis, M. I., Huang, M., Leitzell, K., Lonnoy, E.,
652 Matthews, J. B. R., Maycock, T. K., Waterfield, T., Yelekçi, O., Yu, R., and Zhou, B. (eds.): Cambridge
653 University Press, Cambridge, United Kingdom and New York, NY, USA, 423–552, 2021. DOI:
654 10.1017/9781009157896.009
655
- 656 Gilbert, D., Rabalais, N. N., Diaz, R. J., & Zhang, J.: Evidence for greater oxygen decline rates in the coastal
657 ocean than in the open ocean. *Biogeosciences*, 7(7), 2283-2296, 2010. DOI: 10.5194/bg-7-2283-2010
658
- 659 Gillibrand, P. A., Cage, A. G., and Austin, W. E. N.: A preliminary investigation of basin water response to
660 climate forcing in a Scottish fjord: evaluating the influence of the NAO. *Continental Shelf Research*, 25(5-6),
661 571-587, 2005. DOI: 10.1016/j.csr.2004.10.011
662
- 663 Grose, M. R., Barnes-Keoghan, I., Corney S. P., White C. J., Holz, G.K., Bennett, J. B., Gaynor, S.M. and
664 Bindof, N.L.: Climate Futures for Tasmania: general climate impacts technical report, Antarctic Climate &
665 Ecosystems Cooperative Research Centre, Hobart, Tasmania, 2010. ISBN: 978-1-921197-05-5
666
- 667 Hartstein, N. D., Maxey, J. D., Loo, J. C. H., and Then, A. Y. H.: Drivers of deep water renewal in Macquarie
668 Harbour, Tasmania. *Journal of Marine Systems*, 199(103226), 2019. DOI: 10.1016/j.jmarsys.2019.103226
669
- 670 Hashimoto, L. K., Kaplan, W. A., Wofsy, S. C., and McElroy, M. B.: Transformations of fixed nitrogen and
671 N₂O in the Cariaco Trench. *Deep Sea Research Part A. Oceanographic Research Papers*, 30(6), 575-590, 1983.
672 DOI: 10.1016/0198-0149(83)90037-7
673
- 674 Hendzel, L. L., Matthews, C. J. D., Venkiteswaran, J. J., St. Louis, V. L., Burton, D., Joyce, E. M., and Bodaly,
675 R. A.: Nitrous oxide fluxes in three experimental boreal forest reservoirs. *Environmental Science & Technology*,
676 39(12), 4353-4360, 2005. DOI: 10.1021/es049443j
677
- 678 Huang, Y., Song, B., Zhang, Q., Park, Y., Wilson, S. J., Tobias, C. R., and An, S.: Seawater intrusion effects on
679 nitrogen cycling in the regulated Nakdong River Estuary, South Korea. *Frontiers in Marine Science*.
680 11(1369421), 2024. DOI: 10.3389/fmars.2024.1369421
681
- 682 Inall, M. E., & Gillibrand, P. A.: The physics of mid-latitude fjords: a review. Geological Society, London,
683 Special Publications. 344(1), 17-33, 2010. DOI: 10.1144/SP344.3
684
- 685 Ji, Q., Jameson, B. D., Juniper, S. K., and Grundle, D. S.: Temporal and vertical oxygen gradients modulate
686 nitrous oxide production in a seasonally anoxic fjord: Saanich Inlet, British Columbia. *Journal of Geophysical
687 Research: Biogeosciences*, 125(9), 2020. DOI: 10.1029/2020JG005631
688



- 689 Kallert, J.: Verteilung von Lachgas (N₂O) und Methan (CH₄) im Fluss Rajang (Malaysia). Bachelor thesis,
690 Christian-Albrecht-University, Kiel, 2017. URI: <https://oceanrep.geomar.de/id/eprint/40913/>
691
- 692 Kock, A. and Bange, H. W.: Counting the ocean's greenhouse gas emissions, *Eos: Earth & Space Science News*,
693 96(3), 10–13, 2015. DOI:10.1029/2015EO023665
694
- 695 Kuypers, M. M. M., Marchant, H. K., and Kartal, B.: The microbial nitrogen-cycling network, *Nature Reviews*
696 *Microbiology*, 16, 263-276, 2018. DOI: 10.1038/nrmicro.2018.9
697
- 698 Laffoley, D., and Baxter, J. M.: Ocean deoxygenation: Everyone's problem: Causes, impacts, consequences and
699 solutions: Summary for Policy Makers. International Union for Conservation of Nature (IUCN), 2019. DOI:
700 10.2305/IUCN.CH.2019.13.en
701
- 702 Lucieer, V.: SeaMap Tasmania Bathymetric Data [data set], Institute for Marine and Antarctic Studies,
703 University of Tasmania, 2007. ISBN: 0-7246-8011-X
704
- 705 Ma, X., Lennartz, S. T., and Bange, H. W. : A multi-year observation of nitrous oxide at the Boknis Eck Time
706 Series Station in the Eckernförde Bay (southwestern Baltic Sea). *Biogeosciences*, 16(20), 4097-4111, 2019.
707 DOI: 10.5194/bg-16-4097-2019
708
- 709 Macquarie Harbour Dissolved Oxygen Working Group (October 2014), Final Report to the Tasmanian Salmonid
710 Growers Association, 2014.
711
- 712 Maher, D. T., J. Z. Sippo, D. R. Tait, C. Holloway, and Santos, I. R.: Pristine mangrove creek waters are a sink
713 of nitrous oxide. *Scientific Reports*, 6(25701), 2016. DOI: 10.1038/srep25701
714
- 715 Manning, C. C., Hamme, R. C., & Bourbonnais, A.: Impact of deep-water renewal events on fixed nitrogen loss
716 from seasonally-anoxic Saanich Inlet. *Marine Chemistry*, 122(1), 1–10, 2010. DOI:
717 10.1016/j.marchem.2010.08.002
718
- 719 Maxey, J. D., Hartstein, N. D., Penjinus, D., & Kerroux, A.: Simple quality control technique to identify
720 dissolved oxygen diffusion issues with biochemical oxygen demand bottle incubations. *Borneo Journal of*
721 *Marine Science and Aquaculture (Bjomsa)*, 1, 2017. DOI: 10.51200/bjomsa.v1i.995
722
- 723 Maxey, J. D., Hartstein, N. D., Then, A. Y. H., and Barrenger, M.: Dissolved oxygen consumption in a fjord-like
724 estuary, Macquarie Harbour, Tasmania. *Estuarine, Coastal and Shelf Science*, 246(107016), 2020. DOI:
725 10.1016/j.ecss.2020.107016
726



- 727 Maxey, J. D., Hartstein, N. D., Mujahid, A., & Müller, M.: The influence of mesoscale climate drivers on
728 hypoxia in a fjord-like deep coastal inlet and its potential implications regarding climate change: examining a
729 decade of water quality data. *Biogeosciences*, 19(13), 3131-3150, 2022. DOI: 10.5194/bg-19-3131-2022
730
- 731 McMahon, P. B., and Dennehy, K. F.: N₂O emissions from a nitrogen-enriched river. *Environmental Science &*
732 *Technology*, 33(1), 21-25, 1999. DOI: 10.1021/es980645n
733
- 734 Michiels, C. C., Huggins, J. A., Giesbrecht, K. E., Spence, J. S., Simister, R. L., Varela, D. E., Hallam, S. J.,
735 Crowe, S. A.: Rates and pathways of N₂ production in a persistently anoxic fjord: Saanich Inlet, British
736 Columbia. *Frontiers in Marine Science*, 6(27), 2019. DOI: 10.3389/fmars.2019.00027
737
- 738 Mickett, J. B., Gregg, M. C., and Seim, H. E.: Direct measurements of diapycnal mixing in a fjord reach—Puget
739 Sound's Main Basin. *Estuarine, Coastal and Shelf Science*, 59(4), 539-558, 2004. DOI:
740 10.1016/j.ecss.2003.10.009
741
- 742 Murray, R. H., Erler, D. V., and Eyre, B. D.: Nitrous oxide fluxes in estuarine environments: response to global
743 change. *Global Change Biology*, 21(9), 3219-3245, 2015. DOI: 10.1111/gcb.12923
744
- 745 Musenze, R. S., U. Werner, A. Grinham, J. Udy, and Z. Yuan.: Methane and nitrous oxide emissions from a
746 subtropical estuary (the Brisbane River estuary, Australia). *Science of the Total Environment*, 472, 719–729,
747 2014. DOI: 10.1016/j.scitotenv.2013.11.085
748
- 749 Myhre, G., Shindell, D., Bréon, F. M., Collins, W., Fuglestedt, J., Huang, J., Koch, D., Lamarque, J. F., Lee,
750 D., Mendoza, B., Nakajima, T., Robock, A., Stephens, G., Takemura, T., and Zhang, H.: Anthropogenic and
751 Natural Radiative Forcing. In: *Climate Change 2013: The Physical Science Basis. Contribution of Working*
752 *Group I to the Fifth Assessment Report of the Intergovernmental Panel on Climate Change* [Stocker, T.F., Qin,
753 D., Plattner, G. K., Tignor, M., Allen, S. K., Boschung, J., Nauels, A., Xia, Y., Bex, V., and Midgley, P. M.
754 (eds.)]. Cambridge University Press, Cambridge, United Kingdom and New York, NY, USA, 2013. DOI:
755 10.1017/CBO9781107415324.018
756
- 757 Myllykangas, J. P., Jilbert, T., Jakobs, G., Rehder, G., Werner, J., and Hietanen, S.: Effects of the 2014 major
758 Baltic inflow on methane and nitrous oxide dynamics in the water column of the central Baltic Sea. *Earth System*
759 *Dynamics*, 8(3), 817-826, 2017. DOI: 10.5194/esd-8-817-2017
760
- 761 Nevison, C., and Holland, E.: A reexamination of the impact of anthropogenically fixed nitrogen on atmospheric
762 N₂O and the stratospheric O₃ layer. *Journal of Geophysical Research: Atmospheres*, 102(D21), 25519-25536,
763 1997. DOI: 10.1029/97JD02391
764
- 765 Orif, M. I., Yasar N. K., Radwan K. A., and Sudheesh, V.: Deoxygenation turns the coastal Red Sea lagoons into
766 sources of nitrous oxide. *Marine Pollution Bulletin* 189(114806), 2023. DOI: 10.1016/j.marpolbul.2023.114806



767

768 Portmann, R. W., Daniel, J. S., and Ravishankara, A. R.: Stratospheric ozone depletion due to nitrous oxide:
769 influences of other gases. *Philosophical Transactions of the Royal Society B*, 367, 1256–1264, 2012. DOI:
770 10.1098/rstb.2011.0377

771

772 Raes, E. J., Bodrossy, L., Van de Kamp, J., Holmes, B., Hardman-Mountford, N., Thompson, P. A., McInnes, A.
773 S., Waite, A. M.: Reduction of the powerful greenhouse gas N₂O in the South-Eastern Indian Ocean. *PLoS One*,
774 11(1), 2016. DOI: 10.1371/journal.pone.0145996

775

776 Ravishankara, A. R., Daniel, J. S., and Portmann, R. W.: Nitrous oxide (N₂O): the dominant ozone-depleting
777 substance emitted in the 21st century. *Science*, 326(5949), 123-125, 2009. DOI: 10.1126/science.1176985

778

779 Raymond, P. A., and Cole, J. J.: Gas exchange in rivers and estuaries: Choosing a gas transfer velocity.
780 *Estuaries*, 24(2), 312-317, 2001. DOI: 10.2307/1352954

781

782 Reading, M. J., Santos, I. R., Maher, D. T., Jeffrey, L. C., and Tait, D. R.: 2017. Shifting nitrous oxide
783 source/sink behaviour in a subtropical estuary revealed by automated time series observations. *Estuarine, Coastal
784 and Shelf Science*, 194: 66-76, 2017. DOI: 10.1016/j.ecss.2017.05.017

785

786 Reading, M. J., Tait, D. R., Maher, D. T., Jeffrey, L. C., Looman, A., Holloway, C., Shishaye, H. A., Barron, S.
787 and Santos, I. R.: Land use drives nitrous oxide dynamics in estuaries on regional and global scales. *Limnology
788 and Oceanography*, 65(8), 1903-1920, 2020. DOI: 10.1002/lno.11426

789

790 Reading, M.J.: Aquatic nitrous oxide dynamics from rivers to reefs. Doctoral dissertation, Southern Cross
791 University, 2022. DOI: 10.25918/thesis.197

792

793 Rönner, U.: Distribution, production and consumption of nitrous oxide in the Baltic Sea. *Geochimica et
794 Cosmochimica Acta*, 47(12), 2179-2188, 1983. DOI: 10.1016/0016-7037(83)90041-8

795

796 Rosentreter, J. A., Wells, N. S., Ulseth, A. J., and Eyre, B. D.: Divergent gas transfer velocities of CO₂, CH₄, and
797 N₂O over spatial and temporal gradients in a subtropical estuary. *Journal of Geophysical Research:
798 Biogeosciences*, 126(10), 2021. DOI: 10.1029/2021JG006270

799

800 Rosentreter, J.A., Laruelle, G.G., Bange, H.W., Bianchi, T.S., Busecke, J.J., Cai, W.J., Eyre, B.D., Forbrich, I.,
801 Kwon, E.Y., Maavara, T. and Moosdorf, N.: Coastal vegetation and estuaries are collectively a greenhouse gas
802 sink. *Nature Climate Change*, 13(6), 579-587, 2023. DOI: 10.1038/s41558-023-01682-9

803

804 Sánchez-Rodríguez, J., Sierra, A., Jiménez-López, D., Ortega, T., Gómez-Parra, A., and Forja, J.: Dynamic of
805 CO₂, CH₄ and N₂O in the Guadalquivir estuary. *Science of The Total Environment*, 805, 2022. DOI:
806 10.1016/j.scitotenv.2021.150193



807

808 Schulz, G., Sanders, T., Voynova, Y. G., Bange, H. W., and Dähnke, K.: Seasonal variability of nitrous oxide
809 concentrations and emissions in a temperate estuary. *Biogeosciences*, 20(15), 3229-3247, 2023. DOI:
810 10.5194/bg-20-3229-2023

811

812 Schweiger, B.: Messung von NH_2OH in ausgewählten Seegebieten. Master thesis, Leibniz Institute of Marine
813 Science, Kiel (IFM-GEOMAR), 2006.

814

815 Seitzinger, S. P., Kroeze, C., and Styles, R. V.: Global distribution of N_2O emissions from aquatic systems:
816 natural emissions and anthropogenic effects. *Chemosphere-Global Change Science*, 2(3-4), 267-279, 2000. DOI:
817 10.1016/S1465-9972(00)00015-5

818

819 Sierra, A., Jiménez-López, D., Ortega, T., Gómez-Parra, A., and Forja, J.: Factors controlling the variability and
820 emissions of greenhouse gases (CO_2 , CH_4 and N_2O) in three estuaries of the Southern Iberian Atlantic Basin
821 during July 2017. *Marine Chemistry*, 226(103867), 2020. DOI: 10.1016/j.marchem.2020.103867

822

823 Salamena, G. G., Whinney, J. C., Heron, S. F., and Ridd, P. V.: Internal tidal waves and deep-water renewal in a
824 tropical fjord: Lessons from Ambon Bay, eastern Indonesia. *Estuarine, Coastal and Shelf Science*, 253(107291),
825 2021. DOI: 10.1016/j.ecss.2021.107291

826

827 Salamena, G. G., Whinney, J. C., Heron, S. F., and Ridd, P. V.: Frontogenesis and estuarine circulation at the
828 shallow sill of a tropical fjord: Insights from Ambon Bay, eastern Indonesia. *Regional Studies in Marine Science*,
829 56(102696), 2022. DOI: 10.1016/j.rsma.2022.102696

830

831 Smith, R. W., Bianchi, T. S., Allison, M., Savage, C., and Galy, V.: High rates of organic carbon burial in fjord
832 sediments globally, *Nature Geoscience*, 8(6), 450-453, 2015. DOI: 10.1038/ngeo2421

833

834 Stow, C. A., Walker, J. T., Cardoch, L., Spence, P., and Geron, C.: N_2O emissions from streams in the Neuse
835 River watershed, North Carolina. *Environmental Science & Technology*, 39(18), 6999-7004, 2005. DOI:
836 10.1021/es0500355

837

838 Sturm, K., Werner, U., Grinham, A., and Yuan, Z.: Tidal variability in methane and nitrous oxide emissions
839 along a subtropical estuarine gradient. *Estuarine, Coastal and Shelf Science*, 192, 159-169, 2017. DOI:
840 10.1016/j.ecss.2017.04.027

841

842 Suntharalingam, P., and Sarmiento, J. L.: Factors governing the oceanic nitrous oxide distribution: Simulations
843 with an ocean general circulation model. *Global Biogeochemical Cycles*, 14(1), 429-454, 2000. DOI:
844 10.1029/1999GB900032

845



- 846 Tait, D. R., Maher, D. T., Wong, W., Santos, I. R., Sadat-Noori, M., Holloway, C., and Cook, P. L. M.:
847 Greenhouse gas dynamics in a salt-wedge estuary revealed by high resolution cavity ringdown spectroscopy
848 observations. *Environmental Science & Technology*, 51: 13771–13778, 2017. DOI: 10.1021/acs.est.7b04627
849
- 850 Teasdale, P. R., Apte, S. C., Ford, P. W., Batley, G. E., and Koehnken, L.: Geochemical cycling and speciation
851 of copper in waters and sediments of Macquarie Harbour, Western Tasmania. *Estuarine, Coastal and Shelf
852 Science*, 57(3), 475-487, 2003. DOI: 10.1016/S0272-7714(02)00381-5
853
- 854 Walinsky, S. E., Prah, F. G., Mix, A. C., Finney, B. P., Jaeger, J. M., and Rosen, G. P.: Distribution and
855 composition of organic matter in surface sediments of coastal Southeast Alaska, *Continental Shelf Research*,
856 29(13), 1565-1579, 2009. DOI: 10.1016/j.csr.2009.04.006
857
- 858 Walter, S., Bange, H. W., and Wallace, D. W.: Nitrous oxide in the surface layer of the tropical North Atlantic
859 Ocean along a west to east transect. *Geophysical Research Letters*, 31(23), 2004. DOI: 10.1029/2004GL019937
860
- 861 Walter, S., Breitenbach, U., Bange, H. W., Naucsh, G., and Wallace, D. W. R.: Distribution of N₂O in the Baltic
862 Sea during transition from anoxic to oxic conditions. *Biogeosciences*, 3, 557-570, 2006. DOI: 10.5194/bg-3-557-
863 2006
864
- 865 Wan, X. S., Lin, H., Ward, B. B., Kao, S., and Dai M.: Significant seasonal N₂O dynamics revealed by multi-
866 year observations in the Northern South China Sea. *Global Biogeochemical Cycles*, 36(10), 2022. DOI:
867 10.1029/2022GB007333
868
- 869 Weiss, R. F. and Price, B. A.: Nitrous oxide solubility in water and seawater, *Marine Chemistry*, 8, 347-359,
870 1980. DOI: 10.1016/0304-4203(80)90024-9
871
- 872 Wells, N. S., Maher, D. T., Erler, D. V., Hipsey, M., Rosentreter, J. A., and Eyre, B. D.: Estuaries as sources and
873 sinks of N₂O across a land use gradient in subtropical Australia. *Global Biogeochemical Cycles*, 32, 877–894,
874 2918. DOI: 10.1029/2017GB005826
875
- 876 Willis, M.: Tascatch Variation 2 – Surface Water Models (Document ID Number WR 2008/005). Department of
877 Primary Industries and Water. Hydro Tasmania Consulting, [https://nre.tas.gov.au/water/water-monitoring-and-
878 assessment/hydrological-assessment/tasmanian-catchmentsmodelling/surface-water-models](https://nre.tas.gov.au/water/water-monitoring-and-assessment/hydrological-assessment/tasmanian-catchmentsmodelling/surface-water-models). 2008.
879
- 880 Wilson, S. T., Bange, H. W., Arévalo-Martínez, D. L., Barnes, J., Borges, A. V., Brown, I., Bullister, J. L.,
881 Burgos, M., Capelle, D. W., Casso, M., de la Paz, M., Farías, L., Fenwick, L., Ferrón, S., García, G., Glockzin,
882 M., Karl, D. M., Kock, A., Laperriere, S., Law, C. S., Manning, C. C., Marriner, A., Myllykangas, J. P., Pohlman,
883 J. W., Rees, A. P., Santoro, A. E., Tortell, P. D., Upstill-Goddard, R. C., Wisegarver, D. P., Zhang, G. L., and
884 Rehder, G.: An intercomparison of oceanic methane and nitrous oxide measurements, *Biogeosciences*, 15, 5891-
885 5907, 2018. DOI: 10.5194/bg-15-5891-2018



886

887 Wilson, S. T., Al-Haj, A. N., Bourbonnais, A., Frey, C., Fulweiler, R. W., Kessler, J. D., Marchant, H. K.,
888 Milucka, J., Ray, N. E., Suntharalingham, P., Thornton, B. F., Upstill-Goddard, R. C., Weber, T. S., Arévalo-
889 Martínez, D. L., Bange, H. W., Benway, H. M., Bianchi, D., Borges, A. V., Chang, B. X., Crill, P. M., del Valle,
890 D. A., Fariás, L., Joye, S. B., Kock, A., Labidi, J., Manning, C. C., Pohlman, J. W., Rehder, G., Sparrow, K. J.,
891 Tortell, P. D., Treude, T., Valentine, D. L., Ward B. B., Yang, S., and Yurganov, L. N.: Ideas and perspectives:
892 A strategic assessment of methane and nitrous oxide measurements in the marine environment. *Biogeosciences*,
893 17, 5809-5828, 2020. DOI: 10.5194/bg-17-5809-2020

894

895 Wu, L., Chen X., Wei, W., Liu, Y., Wang, D., and Ni, B.: A critical review on nitrous oxide production by
896 ammonia-oxidizing archaea. *Environmental Science & Technology* 54(15), 9175-9190, 2020. DOI:
897 10.1021/acs.est.0c03948

898

899 Yevenes, M. A., Bello, E., Sanhueza-Guevara, S., and Fariás, L.: Spatial distribution of nitrous oxide (N₂O) in
900 the Reloncaví estuary–sound and adjacent sea (41–43 S), Chilean Patagonia. *Estuaries and Coasts*, 40, 807-821,
901 2017. DOI: 10.1007/s12237-016-0184-z

902

903 Yoshinari, T.: Nitrous oxide in the sea. *Marine Chemistry* 2(4), 189–202, 1976. DOI: 10.1016/0304-
904 4203(76)90007-4.

905

906 Zappa, C. J., Raymond, P. A., Terray, E. A., and McGillis, W. R.: Variation in surface turbulence and the gas
907 transfer velocity over a tidal cycle in a macro-tidal estuary. *Estuaries*, 26, 1401-1415, 2003. DOI:
908 10.1007/BF02803649

909

910 Zhang, G. L., Zhang, J., Liu, S. M., Ren, J. L., and Zhao, Y. C.: Nitrous oxide in the Changjiang (Yangtze
911 River) Estuary and its adjacent marine area: Riverine input, sediment release and atmospheric fluxes.
912 *Biogeosciences* 7(11), 3505-3516, 2010. DOI: 10.5194/bg-7-3505-2010